1990   Thesis/Dissertation

Lightning Ground Strikes Analyzed by Singularity and
Fractal Techniques: A Mesoscale Convective Complex
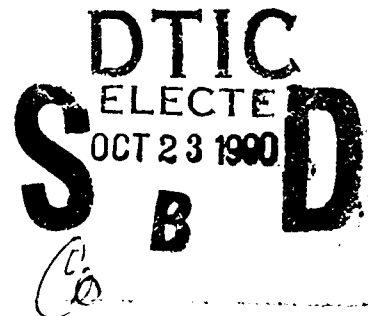Study

Daniel Bruce Frashier

AFIT Student at: University of Oklahoma

AFIT/CI/CIA – 90-080

AFIT/CI
Wright-Patterson AFB OH 45433

DTIC
ELECTE
OCT 23 1990
B

105

UNCLASSIFIED

THE UNIVERSITY OF OKLAHOMA

GRADUATE COLLEGE

LIGHTNING GROUND STRIKES ANALYZED BY

SINGULARITY AND FRACTAL TECHNIQUES:

A MESOSCALE CONVECTIVE COMPLEX

CASE STUDY

A THESIS

SUBMITTED TO THE GRADUATE FACULTY

in partial fulfillment of the requirements for the

degree of

MASTER OF SCIENCE IN METEOROLOGY

By

DANIEL BRUCE FRASHIER

Norman, Oklahoma

1990

LIGHTNING GROUND STRIKES ANALYZED BY

SINGULARITY AND FRACTAL TECHNIQUES:

A MESOSCALE CONVECTIVE COMPLEX

CASE STUDY

A THESIS

APPROVED FOR THE SCHOOL OF METEOROLOGY

By

Donald R MacGorman

William H. Beasley

ACKNOWLEDGEMENTS

Special thanks goes to my loving wife, Chong Sun, for
her understanding and strength throughout the last two
years. Her support was vital to the completion of this
endeavor. Also, love and thanks go to my daughter Sarah
Kim, who was born during this study, for understanding why
daddy was so busy and couldn't play with her. I pray that I
can make it up to them both. To Mom and Father Bear, thanks
from the bottom of my heart. Your support and guidance
through the years have made me what I am today.

Above all, I want to thank my eternal Lord and Savior,
Jesus Christ, who died so that I might live. Through grace,
he has freed me from sin, given me the gift of eternal life,
and made me complete.

TABLE OF CONTENTS

LIST OF TABLES

LIST OF ILLUSTRATIONS

ABSTRACT

The relationship between thunderstorm dynamics and lightning strike locations, of both polarities, is examined on the Mesoscale Convective Complex that produced a mesocyclone and gust front on 27 May 1987. Two analysis techniques were used for the first time on this type of lightning data. The first is a singularity analysis using single Doppler radar data obtained from the National Severe Storms Laboratory (NSSL). The lightning data were also obtained from NSSL.

The singularity analysis technique assumes local symmetry to calculate the strength of source/sink (or divergence/convergence) and rotating (or vorticity) singularities using Doppler radar wind data. A time period of two hours and 38 minutes was analyzed with this technique, during which a well defined gust front was located along with a mesocyclone that developed along the gust front. Both features were detected well in advance of corresponding surface reports. Background convergence was also calculated for low levels using the singularity method and was seen to be highly correlated with the number of negative cloud-to-ground lightning strikes. Upper level divergence was also seen in the form of a jet maximum in the Doppler velocities and also correlated favorably with total cloud-to-ground lightning

strikes and low level background convergence. It was also discovered that the singularity technique was able to locate areas of aliased (or folded) velocities within the data set, and may be used to correct (or unfold) the aliased data more accurately. Reliable unfolding techniques are vital for the nation's Next Generation Weather Radar (NEXRAD).

The second analysis method was a fractal technique. The fractal dimension of the ground strike locations was calculated for five hours of data in 30 minute intervals (extending one hour before and after the singularity analysis described above). It was found that the distribution of the lightning ground strikes is a fractal. The fractal was observed, however, for negative ground strikes only. A fractal dimension of negative ground strikes of D=1.21 was found within the main core of lightning activity for 30 minute increments. When the analysis was repeated for a five hour interval, the fractal dimension of negative ground strikes was D=1.7. This is the same fractal dimension that was measured for lightning channels using photographs. Very little fractal presence was found for positive ground strikes. This may be due in part to the relative scarcity of positive ground strikes. When the analysis was repeated for the entire five hour period, the positive strikes still did not show a strong fractal presence. Self-similarity

does not appear to be an inherent trait of positive cloud-to-ground lightning as it is with negative cloud-to-ground lightning.

LIGHTNING GROUND STRIKES ANALYZED BY
SINGULARITY AND FRACTAL TECHNIQUES:
A MESOSCALE CONVECTIVE COMPLEX
CASE STUDY

CHAPTER I

INTRODUCTION

Lightning, one of the most dangerous of all weather
phenomena, has received much attention by researchers in the
past decade or two. Advances in electronics and other tech-
nologies have greatly improved the ability to detect
cloud-to-ground lightning of both polarities and have in-
creased the current level of understanding of this phe-
nomenon. With the establishment of a demonstration national
lightning ground-strike location system, lightning informa-
tion is moving into mainstream meteorology as an additional
forecasting tool. Research into how ground strike informa-
tion can benefit operational meteorologist is becoming in-
creasingly important.

In general, lightning is classified as either intracloud
(*IC*) or cloud-to-ground (*CG*) (MacGorman, 1989). As the
names imply, intracloud lightning is lightning within the

cloud and cloud-to-ground lightning is lightning that joins the cloud to the surface of the Earth. Cloud-to-ground lightning is further subdivided into negative CG lightning and positive CG lightning, the main difference being that negative CG lightning effectively moves negative charge from the cloud to the ground while positive CG lightning effectively moves positive charge from the cloud to the ground (Beasley et al., 1983).

The charge distribution within thunderstorms is generally complex and poorly understood. For many purposes, it is useful to think in terms of the dipole distribution shown in figure 1.1. The main features are the upper positive charge region in the upper portions of the storm and main negative charge region located in the middle portion of the storm. This is generally termed a *positive dipole* which means the positive charge region is above the negative charge region. Between these two regions is where most of the *IC* lightning originates (Mazur et al., 1984). Other areas of interest include the lower positive charge centers (LPCC's) and the screening layer. Some researchers term the upper positive region, the main negative region and the lower positive charge centers as a *tripole* (Williams, 1989). Laboratory studies have shown the importance of the lower positive charge centers in helping to initiate cloud-to-ground lightning (Williams et al., 1985).

Positive cloud-to-ground lightning is rare compared to negative cloud-to-ground and intracloud lightning. Studies of summer thunderstorms have shown that 3-10% of all cloud-to-ground lightning is positive (e.g. Beasley et al., 1983; Fuquay, 1982). However, winter thunderstorms in Japan (Takeuti et al., 1978; Brook et al., 1982) produce mostly +CG flashes (i.e. 90-100%). Takeuti et al. (1978) found that these storms are characterized by strong vertical wind shear. This produces a tilted, or sheared, dipole with the upper positive charge region above and *displaced horizontally* from the main negative charge region. Recent studies have presented support for the tilted dipole hypothesis, as well as suggesting an additional mechanism that is sometimes effective (Williams, 1989; Engholm et al., 1990).

Brook et al. (1982) noted a direct correlation between the percent of +CG flashes and wind shear, with a possible threshold value of 1.5 m/s/km. They also speculated that without wind shear, the positive discharges would result in *IC* lightning and cloud-to-ground lightning would be dominated by negative discharges. This suggests that severe thunderstorms might be candidates for high +CG flash counts due to their highly sheared environment. Rust et al. (1985a) reported on storms that formed along a dryline in the Texas panhandle that had predominately +CG flashes. They also noted that the transition zone between cells with mostly +CG flashes and storms with mostly -CG flashes was where the

vertical shear became less than 2 m/s/km east of the +CG
activity. This value is close to the 1.5 m/s/km reported by
Brook et al. (1982). However, not all severe storms produce
mostly +CG lightning (Rust et al., 1981). Reap and MacGor-
man (1989) showed that, over two warm seasons, the correla-
tion between +CG flashes and wind shear *predictors* was uni-
formly low because shear is high on many days without severe
weather. Predictors such as moisture convergence, low level
vorticity, K stability index (a measure of how convectively
unstable the atmosphere is), low level vertical velocity,
etc. were of more value than wind shear in forecasting prob-
abilities of lightning strikes, of both polarities. They
suggested that high wind shear may be a necessary but not
sufficient condition for +CGs to occur.

Cloud depth also appears to affect +CG strike frequency.
The Japanese winter storms are shallow with cloud tops sel-
dom above 5 km (16,400 ft). Severe storms in the US are
commonly above 18 km (59,000 ft). Reap and MacGorman (1989)
showed that +CG flashes are directly related to storm inten-
sity (i.e. reflectivity or VIP levels). As VIP levels in-
creased, the flash relative frequency for +CGs increased.
On the other hand, Engholm et al. (1990) showed that nega-
tive strike centers are located within the deepest convec-
tion whereas positive strike centers are located in more
shallow convection in winter and summer storms along the
east coast of the United States. A seasonal variability in

4

+CG flashes similar to that found in Japan was observed in the northeast US by Orville et al. (1987) where a 5% +CG flash rate in the summer grew to over 80% in the winter.

Rust et al. (1981) observed that, for an isolated severe thunderstorm, CG flashes of either polarity can emanate from under the upshear anvil on the rear of the storm, from the downshear anvil near the main storm, and from the wall cloud, but most are negative ground strikes. No +CG flashes were observed within precipitation cores. On the other hand, most CG flashes from the downshear anvil well away from the storm tower were positive. Positive cloud-to-ground lightning was observed from squall lines primarily on the rear of the line. They also noted that +CGs can cluster in time. Fuquay (1982) showed that 70% of observed +CGs occurred during the last 10-30 minutes of a mountain storm. This time period was usually void of -CGs but intracloud lightning continued to occur.

A spatial segregation of positive and negative CG strike locations has been observed by Orville et al. (1988) and was termed a *bipole pattern*. This distribution is oriented with the upper level winds, which has little directional shear. Engholm et al. (1990) showed that the bipole was oriented with the geostrophic wind in winter storms and with the vertical wind shear vector, which may be highly ageostrophic, in summer storms. The positive centers are located downwind (or downshear) from the negative center. The dis-

tance between centers, which can be 60-250 km, is much greater than that of individual cells and appears to be a mesoscale feature. Typically, a frontal boundary at the surface separates the positive flash center from the negative flash center. Speed shear for these systems is usually greater than the 1.5 m/s/km suggested by Brook et al. (1982) as a +CG occurrence threshold.

The bipole pattern has been observed in all seasons but favors fall and winter systems and has been observed mostly in the southeast US. It consists of two strike centers throughout most of the several hour life of the storm. Therefore, it is not due to +CGs coming at the decaying stage of the storm as Fuquay (1982) noted. Fuquay (1982) reported on several +CG lightning channels which travelled horizontally for long distances before finally coming to ground. This may explain some of the spatial segregation. Other possible explanations that have been proposed include charge advection and local charge generation (Rutledge and MacGorman, 1988 and 1989). Engholm et al. (1990) also proposed that in situ charging was occurring in the more strat- iform precipitation regions associated with the positive center. However, they concluded that this local generation of charge is fundamentally a convective scale (10-20 km), not mesoscale (>100 km), phenomenon.

A major feature of positive cloud-to-ground lightning is that many have continuing current (CC). Continuing current occurs when current continues to flow in the lightning channel for an extended period of time, 30-240 ms (Rust et al., 1981). Rust et al. (1985b) showed photographic evidence of CC in four out of 36 confirmed +CG flashes. Also, 19 +CGs showed field changes similar to the four with verified CC (i.e. >50% of the observed +CGs had CC). For the winter storms in Japan, Takeuti et al. (1978) reported 67% of the +CG flashes had CC.

The solitary waveform of electric field change from positive cloud-to-ground lightning return strokes appears to be similar to waveforms from negative cloud-to-ground lightning except for the polarity (Beasley et al., 1983). This allows the same direction-finding network to detect both types of CGs (MacGorman and Taylor, 1989).

Most +CG flashes have only one return stroke (Fuquay, 1982; Beasley et al., 1983) but a few +CG flashes have been observed to have two return strokes (Takeuti et al., 1978; Rust et al., 1981; Reap and MacGorman, 1989). Orville et al. (1987) noted that for a full year's worth of data from the northeast US, 90% of all observed +CGs were of the one return stroke type, regardless of season. Negative CGs, on the other hand, had a seasonal variability in multiplicity. Approximately 40% of -CG flashes in June had single return strokes. This increased to 80% by January and fell back to

50% by April. Reap and MacGorman (1989) also reported that negative flashes were much more likely to have multiple strokes than positive flashes in summer storms.

The average peak current for +CG lightning is 40-60 kiloAmperes (kA), well above the mean -CG current of 30 kA (Cooray and Lundquist, 1982). The charge lowered by a +CG flash averages around 100 Coulombs (C), 10 times larger than for -CG flashes. One flash was observed to have a peak current of 100 kA and lowered a total charge of 300 C (Brook et al., 1982). This is partly a result of continuing currents. This has made research into +CGs a hot topic over the last ten years due to their hazards to aircraft and potential for starting forest fires. Table 1 lists some basic characteristics of positive and negative cloud-to-ground lightning.

Cloud-to-ground lightning activity during Mesoscale Convective Complexes (MCCs) has been documented by Goodman and MacGorman (1986). They found that the peak flash rates came, on average for the ten storms sampled, 1.8 hours after initiation, when MCC criteria are first met (Maddox, 1980), 2.6 hours before maximum extent (i.e. maximum extent of the cloud shield as observed by infrared satellite images), and seven hours before termination (i.e. MCC criteria no longer met). However, the total number of ground strikes and the maximum flash rate did not appear to be directly related to cloud shield size or MCC duration. They did note an in-

crease in flash rates as the -52° C cloud area, as seen from infrared satellite images, expanded rapidly. Most of the MCCs they studied had sustained flash rates of >1000 per hour for nine or more hours. This makes an MCC one of the most prolific lightning producers of all storm types. No attempt was made to distinguish between positive and negative cloud-to-ground flashes. Later, Rutledge and MacGorman (1988 and 1989) documented the observations of +CGs within mesoscale convective systems. They found that most of the positive ground strikes were located in the more stratiform precipitation.

Much has been discovered about lightning within the last twenty years. However, much remains to be explained. Positive cloud-to-ground lightning, which is rare but not as rare as once thought, continues to receive much attention due to the large currents carried and the high likelihood of continuing currents.

This study uses two analysis techniques not previously used in lightning research. They are singularity and fractal analyses. Use of both gives us unique insight into the relationships between lightning and other storm features. The main goals of this research are:

1. To determine if singularity analysis provides any useful information to lightning researchers or operational meteorologists. This analysis technique is useful in locating several important meteorological

features. Gust front and mesocyclone identification
is documented in Chapter V. A microburst has also
been observed (Sasaki et al., 1990) as has a tornado
(Sasaki et al., 1989).

2. To determine the existence of a fractal within the
   storm electrical structure. If it exists, does it
   exist for both polarities of cloud-to-ground light-
   ning? Can any information be obtained concerning the
   storm electrical environment, storm charging or dis-
   charge mechanisms, etc. from a fractal analysis?

Table 1. Characteristics of Cloud-to-Ground Lightning		
	+CGs	-CGs
Frequency of occurrence	3-10% *	90-97%
Number of Return Strokes	Usually 1	Usually 3-4, fewer in winter
Continuing Current present	Often	Occasionally
Peak Current (kA)	40-60	30
Charged lowered to ground(C)	+100	-10
Peak Electric Field of First Stroke Normalized to 100 km (volts/meter)	20	18

* Also a seasonal variation with a relatively high percentage of CGs in winter storms being positive.

See text for references.

11
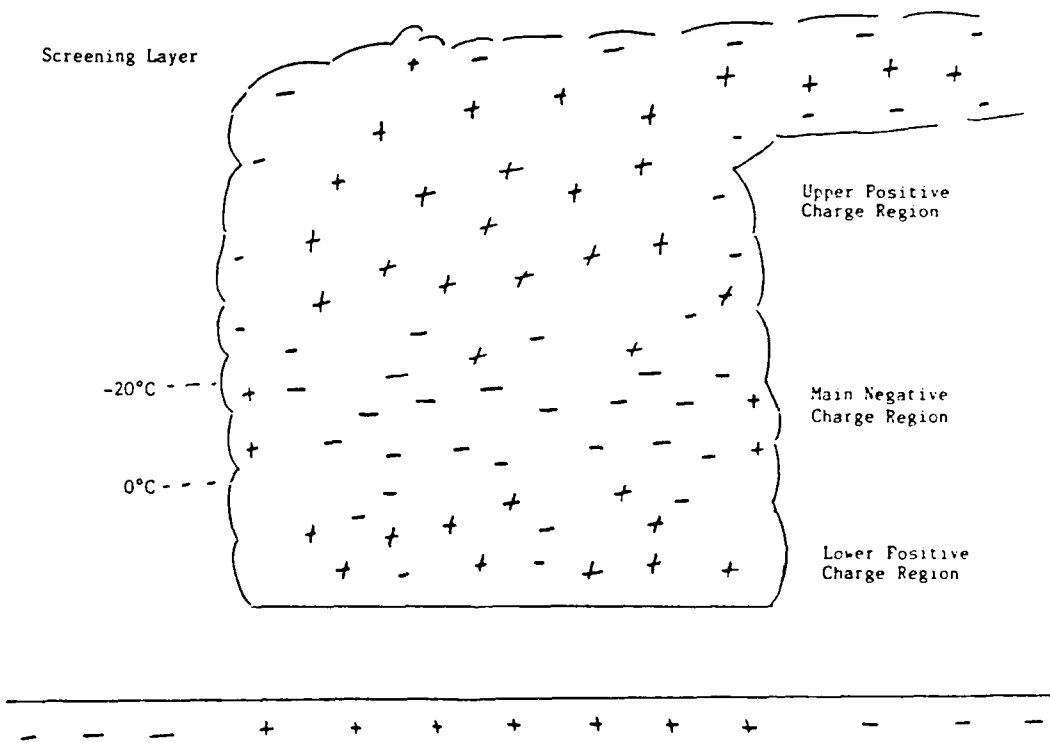
Figure 1.1: Simplified schematic of thunderstorm charge distribution.

CHAPTER II

MCC CASE STUDY

On 27 May, 1987, a thunderstorm complex developed in southwest Texas, near Hobbs, New Mexico, approximately 19 hours before the time-frame analyzed here. At 03Z (2100 CST) on 27 May 87, a dryline extended from a surface low in eastern Colorado through extreme eastern New Mexico into the Big Bend region of Texas (see figure 2.1). The National Meteorological Center (NMC) surface analysis depicts this dryline as a cold front. However, the surface data supports calling it a dryline. For example, temperature/dew point readings at Amarillo, Texas (east of the "front") are 68/65 and at Los Vegas, New Mexico (west of the "front") are 67/28. The initial thunderstorm developed on the dryline east of Hobbs around 02Z (2000 CST) on 27 May and slowly moved north along the dryline (see figures 2.2 and 2.3). By 10Z (0400 CST) on 27 May it had met MCC criteria (Maddox, 1980) and was located in the Texas panhandle (see figure 2.4). At approximately 13Z (0700 CST) it started to move

slowly eastward into western Oklahoma where it became quasi-stationary, progressing eastward very slowly, for the next 19 hours (see figures 2.5-10).

The maximum extent of the cold cloud shield occurred near the end of the analysis time (0130Z - 1930 CST. See figure 2.8). During the termination stage, which began at approximately 08Z (0200 CST) on the 28th, newer convection from the Texas panhandle overtook the remains of the MCC (see figures 2.9-10).

The 12Z (0600 CST) 27 May 87, 500 mb analysis (see figure 2.11) shows a closed low in Wyoming with a longwave trough extending into southern California. A shortwave is embedded within the flow in central Texas. At the same time, the surface analysis (see figure 2.12) shows a surface low in eastern Montana with a warm front into the upper great lakes and a cold front through western Kansas into west Texas. The analysis also depicts the leading edge of our MCC as a squall line from Lubbock to Altus to near Bartlesville, Oklahoma. Gulf moisture is in place across central Texas and Oklahoma eastward into the Ohio river valley.

By 00Z (1800 CST) on 28 May 87, the main trough at 500 mb (see figure 2.13) has rotated into southern Arizona. The shortwave that was in central Texas is now weak and over Wichita, Kansas. A second shortwave is found near Texarkana. The surface analysis has changed little over the

14

last 12, or even 24 hours (see figure 2.14). The squall line is now depicted from Wichita Falls to east of Tulsa to Joplin, Missouri. A precipitation induced High is located over northeastern Oklahoma. The 00Z (1800 CST), 28 May Skew-T diagram for Oklahoma City (see figure 2.15) shows a typical convective sounding, that is, moist adiabatic. Large low level shear is evident along with a low level jet at 700 mb. Also seen is the mid-level warm-core/upper-level cold-core signature noted by Maddox (1983).

During its nearly 30 hour life-cycle, this MCC produced large hail in the Texas panhandle, wind damage along the Kansas/Oklahoma border south of Wichita, and a gust front that moved across the towns of Norman and Noble in Oklahoma. This gust front, and the weak mesocyclone that developed on the northern end of it, will be discussed more in Chapter V. Most notable were the large amounts of precipitation that fell across much of the state of Oklahoma, Chickasha for example, receiving nearly seven (7) inches of rain in a twelve hour period (Cieslik, 1990). Other, unofficial reports indicated that 10-13 inches fell in some locations. This caused flash flooding in many areas. Two people, a 14-year-old boy and a two-year-old girl, drowned (Storm Data). Roads and bridges were washed out ($25 million in damages), homes and businesses were damaged ($10 million) and crops were destroyed ($30 million).
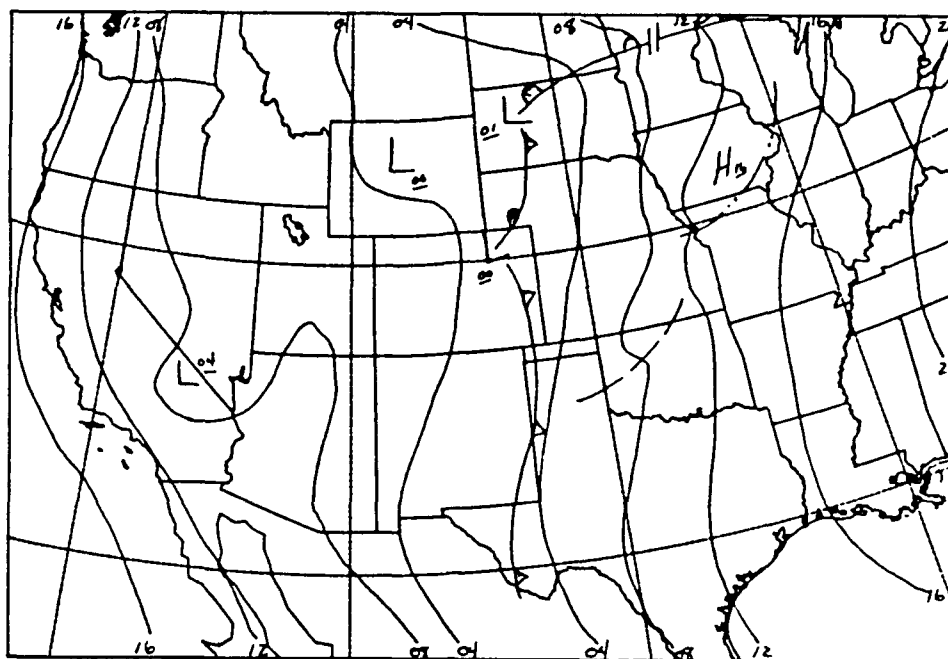
SURFACE ANALYSIS   0300 GMT 27 MAY 1987

Figure 2.1:   Surface analysis for 03Z (2100 CST) on 27 May 1987.

0231 27MY87 29E-2MB 01454 13132 EB2
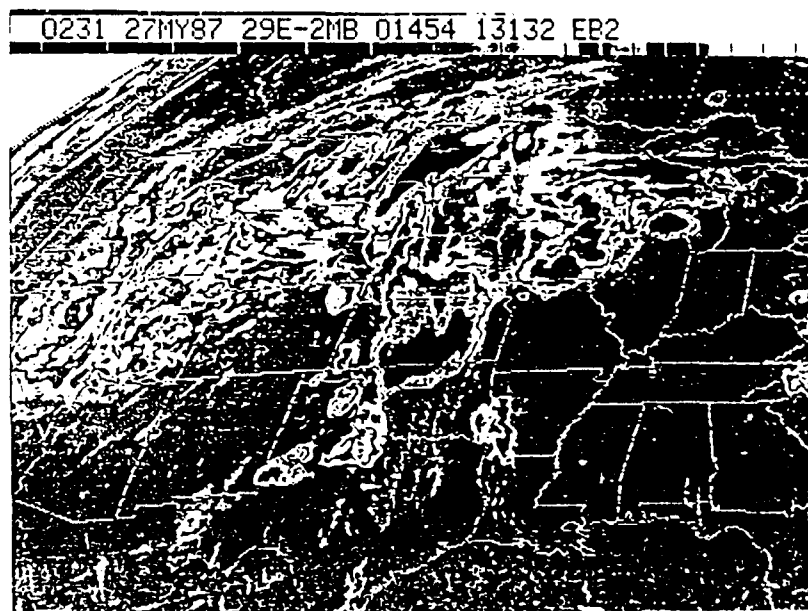
Figure 2.2:   Infrared satellite picture for 0231Z on 27 May,
              1987 (2031 CST on 26 May).

16
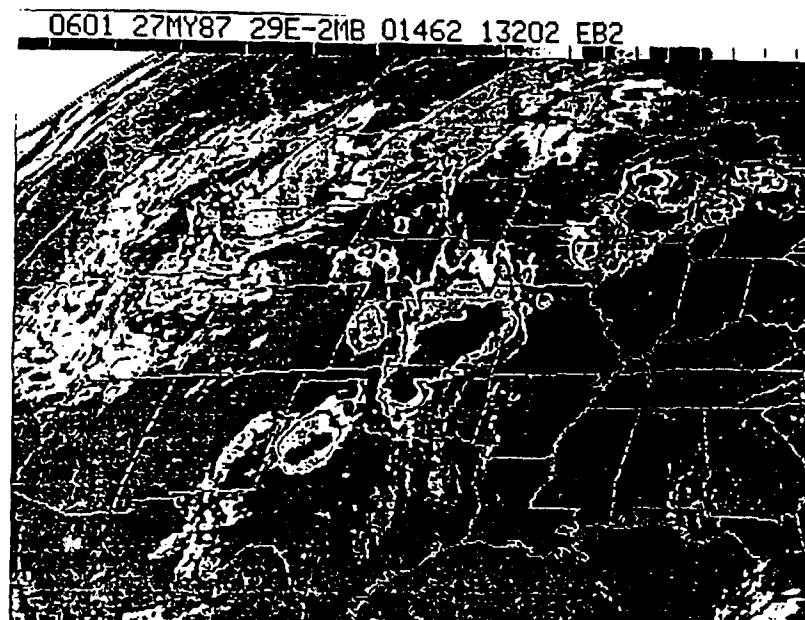
Figure 2.3:   Same as Figure 2.2 except for 0601Z (0001 CST)
on 27 May, 1987.
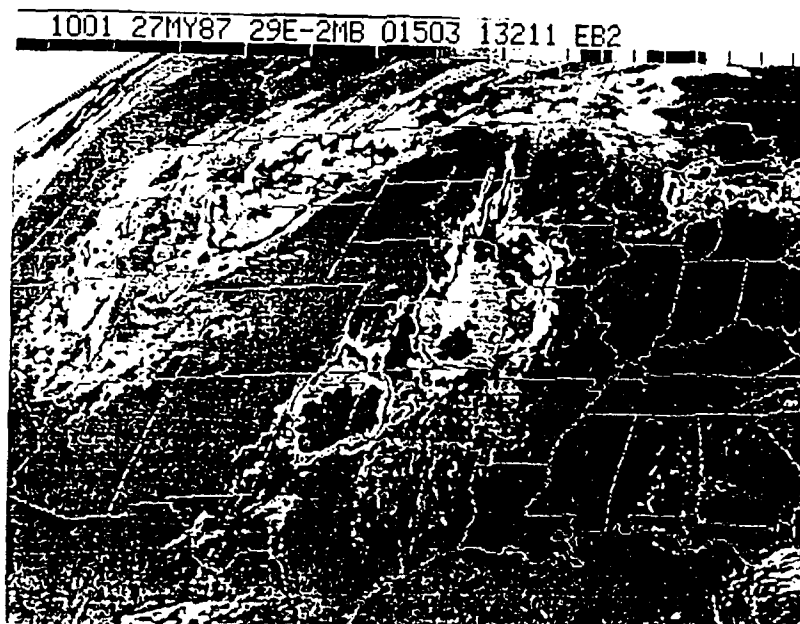
Figure 2.4:   Same as Figure 2.2 except for 1001Z (0401 CST)
on 27 May, 1987.
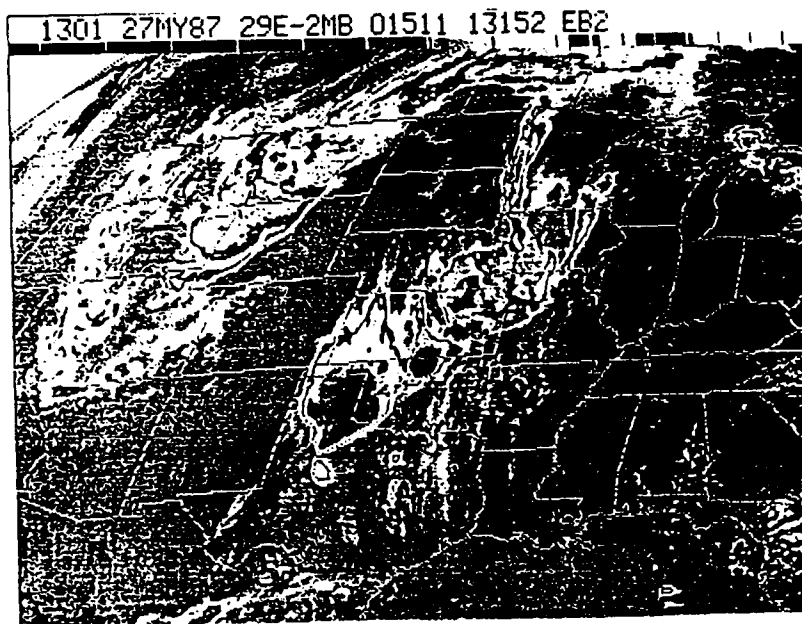
Figure 2.5: Same as Figure 2.2 except for 1301Z (0701 CST) on 27 May, 1987.
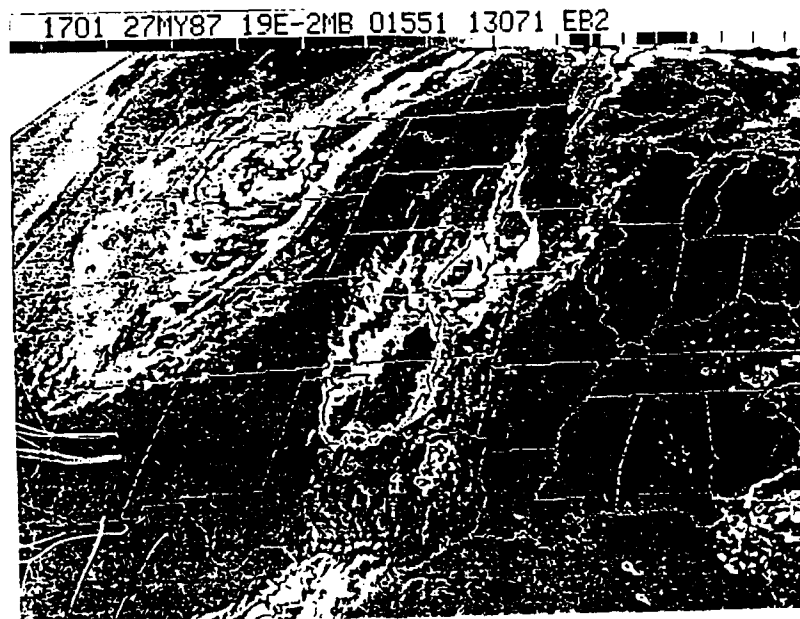
Figure 2.6: Same as Figure 2.2 except for 1701Z (1101 CST) on 27 May, 1987.
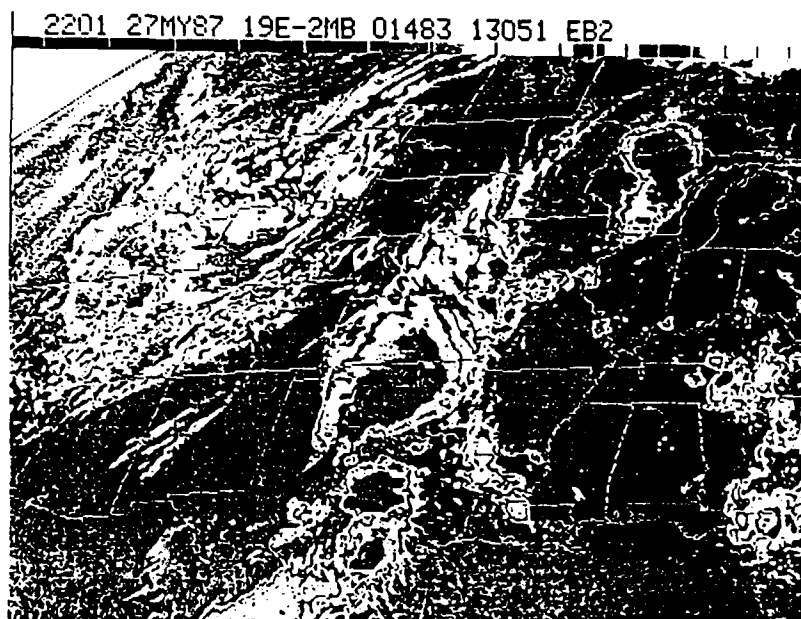
Figure 2.7: Same as Figure 2.2 except for 2201Z (1601 CST) on 27 May, 1987.
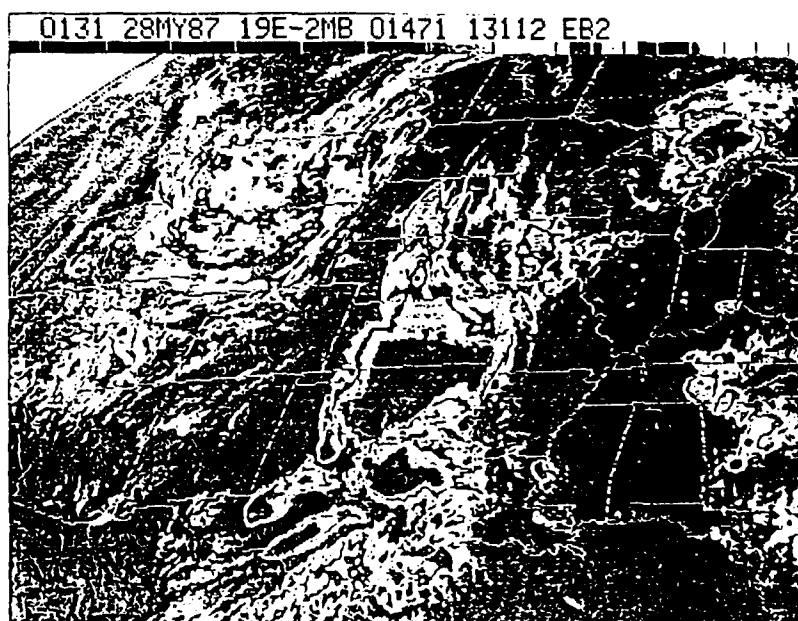
Figure 2.8: Same as Figure 2.2 except for 0131Z on 28 May, 1987 (1931 CST on 27 May).
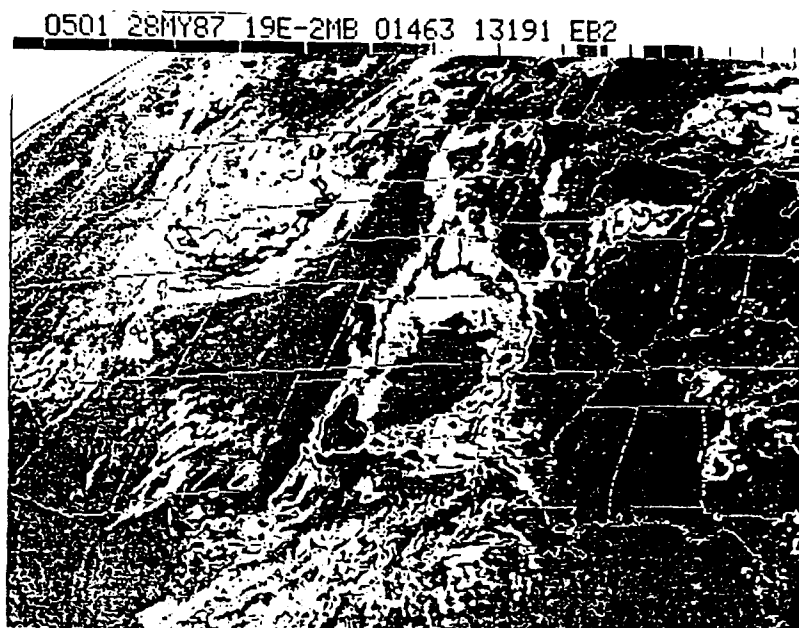
Figure 2.9: Same as Figure 2.2 except for 0501Z on 28 May, 1987 (2301 CST on 27 May).
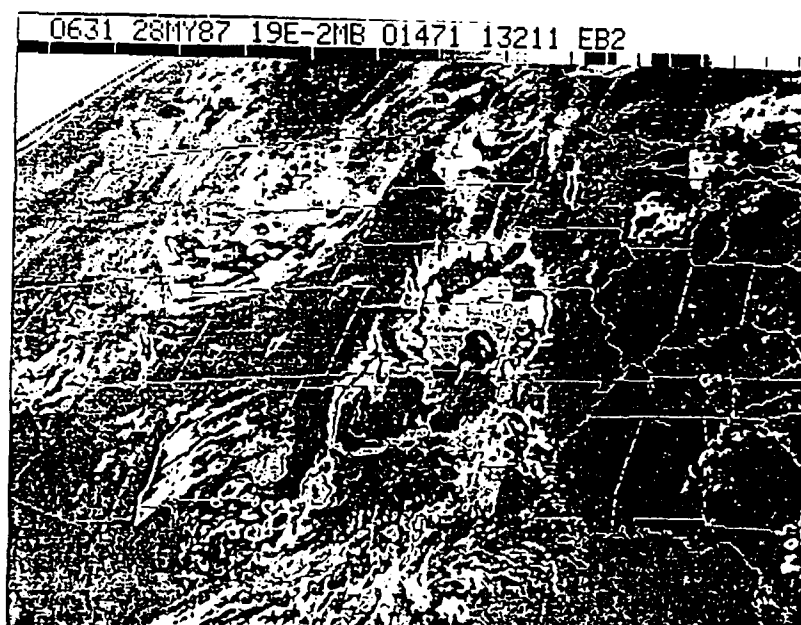
Figure 2.10: Same as Figure 2.2 except for 0631Z (0031 CST) on 28 May, 1987.
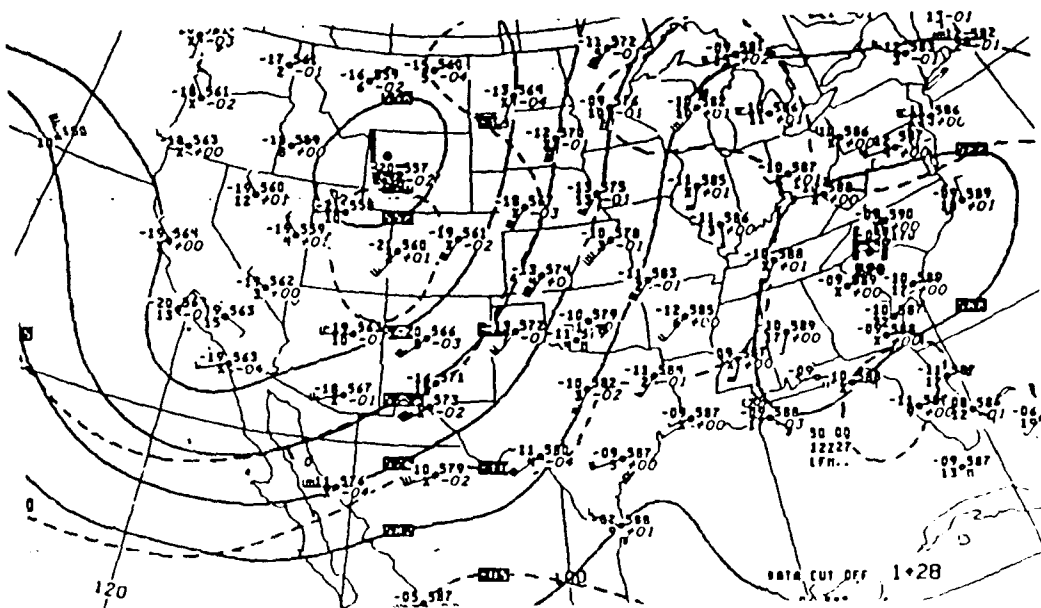
Figure 2.11: 500 mb analysis for 12Z (0600 CST) on 27 May, 1987.

SURFACE ANALYSIS   1200 GMT 27 MAY 1987
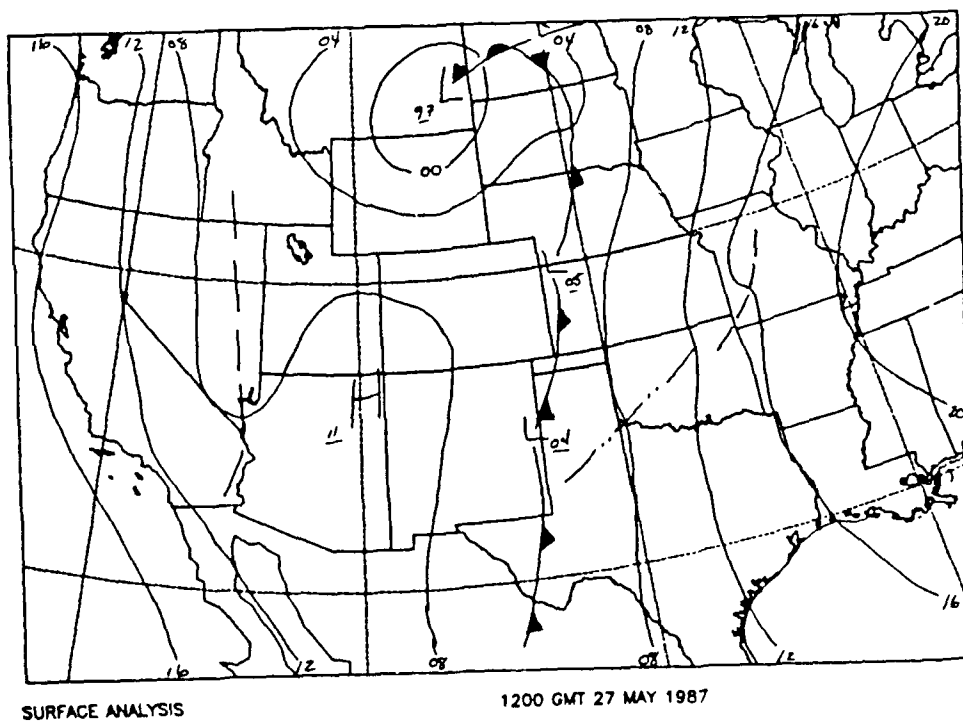
Figure 2.12: Surface analysis for 12Z (0600 CST) on 27 May, 1987.

21
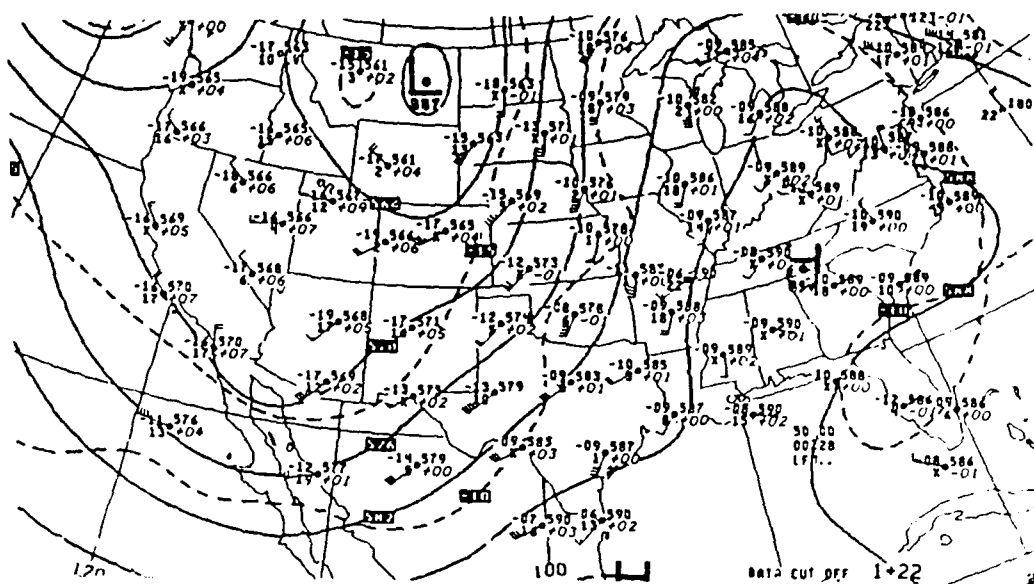
Figure 2.13: 500 mb analysis for 00Z (1800 CST) on 28 May, 1987.

SURFACE ANALYSIS   0000 GMT 28 MAY 1987
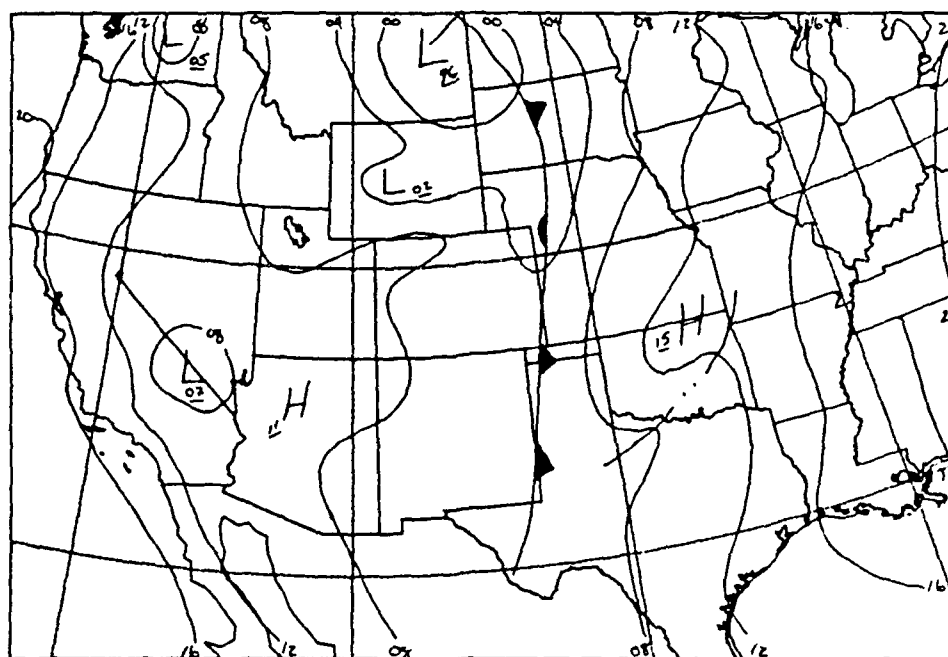
Figure 2.14: Surface analysis for 00Z (1800 CST) on 28 May, 1987.

22
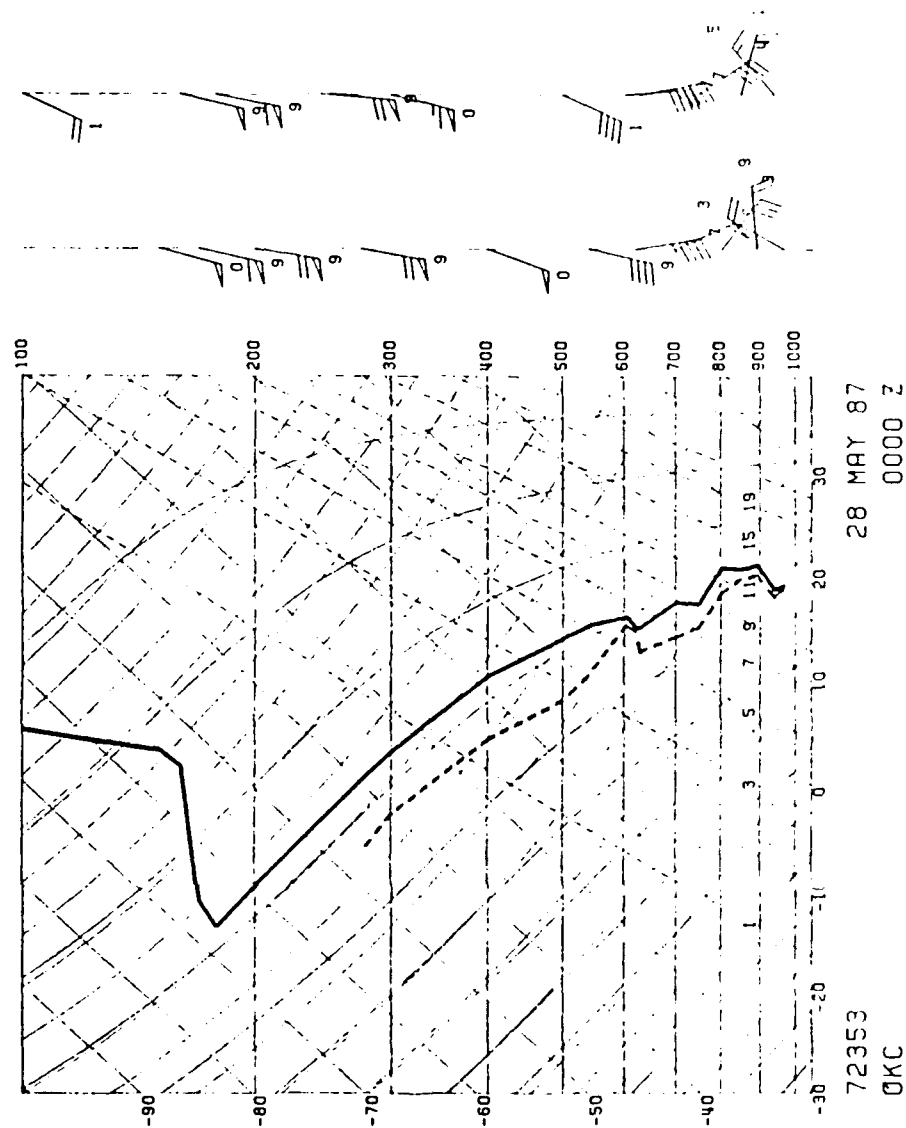
Figure 2.15: Skew-t diagram for Oklahoma City (OKC) at 00Z
(1800 CST) on 28 May, 1987.

CHAPTER III

ANALYSIS TECHNIQUES

A. Singularity

A knowledge of wind velocities in two or three dimensions within a thunderstorm is prerequisite to an understanding of the dynamical structure of the storm. To obtain two-dimensional velocities on a horizontal plane within a storm, you must have two independent forms of information. This information can be the two wind components (U & V) or the vorticity and divergence. The U and V wind components can be obtained from dual-Doppler radar analysis of the radial velocities from both radars. However, the Next Generation Weather Radar (NEXRAD) system scheduled to begin operations in 1991 around the United States, and at select Department of Defense locations around the world, is a single Doppler radar. Single Doppler radars give only one wind component, that is, along the radar beam. Additional information is needed to obtain the two- or three-dimensional wind field from sin-

gle-Doppler radar data.

One possibility is to use a set of equations describing spatial and temporal variations of atmospheric motion. However, this requires high resolution data, in space and time, in a three-dimensional volume of the atmosphere. The resulting computations would be quite expensive and the accuracy of numerical solutions, if they exist, is questionable. The high computational expense makes this method unacceptable for operational use.

Sasaki (1955) introduced the concept of using variational methods for numerical prediction of flow in the atmosphere. In 1983, Sasaki (unpublished work later published as Sasaki et al., 1989) developed, using Green's theory of local symmetry of singularities, a variational method to extract singularities from single Doppler radar data called *DOVES* (**Doppler Operational Variational Extraction of Singularities**). In this research, I have used parts of the *DOVES* analysis to study cloud-to-ground lightning in the mesoscale convective complex (MCC) that occurred on May 27, 1987 in Oklahoma. The two dimensional wind field was not reconstructed in this work. Rather, the singularities were used to identify regions in the storm with significant dynamic activity. One extremely interesting discovery from this analysis is a possible way to identify folded velocities and is discussed in depth in Chapter VI.

A singularity occurs at a point at which the value of
the independent variable is one for which the dependent
variable or function goes to infinity. Since velocity in
the real atmosphere does not go to infinity, we assume a
uniform source strength within a specific radius of the
singularity to avoid the velocity going to infinity at the
singularity point (see figure 3.a.1). Singularities math-
ematically represent complex flows, such as sheared or
rotational flows (Lamb, 1932; Prandtl and Tiejens, 1957;
Milne-Thomson, 1960; Rouse, 1961). A source is visualized
as being uniform, divergent flow outward in all direc-
tions. The source strength is then the total flux outward
across a small closed surface (Lamb, 1932). A sink is
simply a negative source. The resulting velocity poten-
tial due to the source is given by:

$$V = \frac{S}{4\pi r}$$

where V is the velocity, S is the source/sink strength
and r is the distance from the source/sink. *DOVES* works
backwards, using velocities obtained from Doppler radar,
to determine the source strength (S). Similarly, velocity
potential due to a vortex can be shown to be equivalent to
a uniform distribution of double sources (Lamb, 1932).

Figures 3.a.2 and 3.a.3 show schematically the prin-
ciple of *local symmetry* for both source/sink (figure
3.a.2) and rotating singularities (figure 3.a.3). Local

26

symmetry is used as a variational analysis constraint to find the location and intensity of a singularity. Since this method is computationally inexpensive, it is desirable from an operational standpoint.

For source and sink singularities (Source/sink singularities are analogous to divergence and convergence. Hereafter, they will be called divergence/convergence singularities or simply divergence singularities. Likewise, rotation singularities will be called vorticity singularities), local symmetry means that the radial velocities on each side of the singularity (S) along the radar beam are equal and opposite (see figure 3.a.2). Actually, local symmetry says that the radial velocities anywhere on a concentric circle around S have the same magnitude. Due to the limitations of single Doppler radar data mentioned above, **DOVES** uses the velocity along each radar beam. Figure 3.a.1 shows the radial velocities along a radar beam for a singularity. The linear portion from -M to M is from the assumption of uniform source strength. Figure 3.a.2 depicts the divergence case with the convergence case being the same except with the wind toward S.

For the rotational singularity (hereafter called vorticity singularities), local symmetry means that radial velocities on either side of S are equal and opposite (see figure 3.a.3). Again, these points (M & -M) are on concentric circles centered on S. Figure 3.a.1 also shows

the radial velocities along an arc-length of a circle centered between the radar and the singularity. Figure 3.a.3 depictes the cyclonic rotation case with the anticyclonic case being the same except the wind blows clockwise.

The algorithm used in this study is outlined below: Divergence/Convergence Singularities:

1. Raw velocity data are processed one beam at a time. Seven data points along the beam are averaged to give one "new" velocity data point (see figure 3.a.4). This will smooth the velocity data and put them on an approximate one kilometer scale (needed later for the vorticity singularities). Missing data (i.e. 999.) are removed and spectrum width is used as an additional filter (no velocity used if its corresponding spectrum width is >15 m/s).

2. A centered difference is taken around each "new" data point (see figure 3.a.5). This centered difference value is the singularity value.

3. Singularity values are kept in local storage if the value is greater than +/- 0.004 s^{-1} and is within 75 km of the radar. The distance threshold is used to exclude noise in the data beyond 75 km. Background divergence is calculated by averaging all singularities less than +/- 0.006 s^{-1}. Approxi-

mately 25,000 singularity points are used to calcu-
late background divergence. Figure 3.a.6 depicts
an example of convergence singularities.

Vorticity Singularities:

1. Using the averaged velocity data points found in
   the above calculations, a centered difference is
   computed along an arc length for each new radius
   away from the radar (see figure 3.a.7). The dis-
   tance between points used in the centered differ-
   ence must be between 1.75-2.25 km. If the angle to
   meet this requirement is less than than 20°, calcu-
   late the singularity.

2. Singularity values are again put into local storage
   for later display. The 75 km and +/- 0.004 s^{-1}
   thresholds apply here as well. Figure 3.a.8 shows
   an example of cyclonic vorticity singularities.

Advantages of *DOVES* include: 1) The location of many
meteorologically significant events including gust fronts,
mesocyclones, tornadoes and microbursts, 2) The solid the-
oretical foundation (i.e. based on fluid mechanics and
mathematics), 3) The creation of a condensed version of
the velocity data (i.e. 360,000 raw data points condensed
to 50-100 singularity points), 4) The provision of an easy
method of calculating background divergence and 5) The
location of areas within the raw velocity data where fold-

ing may be occurring (see Chapter VI).

Again, for this study, *DOVES* was used as a tool to locate dynamic regions within the MCC and to calculate background divergence which then was correlated to lightning ground strike locations. This, along with the fractal dimension analysis discussed below, may provide additional tools to research and operational meteorologists alike.

B. Fractal

Fractal geometry is a relatively new branch of mathematics. Some fractals came under mathematical scrutiny early in this century. However, it was not until 1975, when the term was coined by Benoit Mandelbrot, that the branch got its name (Barnsley et al., 1988; Blumen et al., 1988). It still remains a little understood curiosity to many research scientists. Advances in fractal theory are being made by applied mathematicians and scientists in chemistry, quantum mechanics, chaos theory, and meteorology.

Some authors flatly refuse to define fractals (Barnsley, 1988). Simply put, fractals are shapes with similar structure at all scales, that is, no characteristic length (Lovejoy, 1982). Fractals, or fractal geometry, is an extension of traditional Euclidean geometry. Where clas-

sical geometry gives us a first approximation of the structure of objects, fractal geometry gives us a more precise model of physical objects (Barnsley et al., 1988). It can describe the intricate details of everything from chemical reactions to galaxies. Euclidean geometric shapes have only a few characteristic length scales or sizes (e.g. radius of a circle or sides of a cube). By contrast, fractals have no characteristic size. Magnifying a fractal gives the same fractal pattern again because of the inherent scale-invarience (i.e. it is self-similar and independent of scale). By contrast, significantly magnifying a traditional geometric object, say a circle, yields a straight line. See figure 3.b.1 for an example of a fractal (the Mandelbrot set) which is magnified eight times.

Several numbers are used to describe fractals. These are generally called *Fractal or Similarity Dimensions*. Where the topographical dimension is an integer, the fractal dimension need not be (Barnsley et al., 1988). The fractal dimension provides a measure of the geometric complexity of the fractal, the wildness of the fractal if you will (Barnsley, 1988). It gives us a "measure" of the size of the fractal in metric space and allows us to compare two fractals. Fractals can be interpreted to give insight into the dynamics of a system. Also, since there

are several ways to calculate the fractal dimension, any discussion of fractal dimensions should explain how the dimension was determined.

Non-integer fractal dimensions can be interpreted as an extension of normal integer dimensions (see figure 3.b.2). An object that is one-dimensional can be divided into N parts that are each scaled by R or $NR^{-1}=1$. A two-dimensional object can be divided into N parts each scaled by R or $NR^{-2}=1$. Likewise for a three-dimensional objected, $NR^{-3}=1$ (Barnsley et al., 1988). This can be generalized into $NR^{-D}=1$. Therefore, the fractal dimension (D) is given by:

$$D = \frac{\log N}{\log R}$$

or

$$\log N = D \log R$$

Therefore, when log (N) is plotted versus log (R), the slope of the resulting line is the fractal dimension (D). In this analysis, N is number of cloud-to-ground lightning strikes and scale ratio, R, is the radius of concentric circles. For *exactly* self-similar curves, such as the von Koch curve, this method of calculating fractal dimension works very well. However, fractals in nature may not be exactly self-similar. A segment of a coastline or a cloud, when magnified, looks like, but not exactly like, segments at different scales. For such *statistically*

self-similar objects, the concept of fractal dimension can still be applied (Barnsley et al., 1988). Note: The derivation shown above is slightly different than one shown in Barnsley et al. (1988) in that R has replaced 1/r. This adjustment adapts better to the method used to calculate the fractal dimensions (D) in this study.

Several investigators have calculated the fractal dimension of clouds, plants, mountains, coastlines, lightning, etc. (e.g. Barnsley et al., 1988; Lovejoy and Schertzer, 1986). Table 2 tabulates some of their findings. These calculations for lightning were done using the box-counting method with photographs of lightning strikes. This fractal dimension measures the fractal associated with that particular discharge, but would not be able to measure the fractal, if one exists, of the storm electrification as a whole. With that in mind, we choose to calculate the fractal dimension of the ground strike locations. The fractal associated with it would be the larger, storm scale fractal. In essence, we would be remotely sensing the organization of electrification within the storm, a task very difficult with present day instrumentation.

A fractal dimensional analysis was conducted on five hours worth of lightning data (1500-2000 CST) from the May 27, 1987 MCC. The basic procedure for calculating the fractal dimension is as follows:

1. Plot lightning ground strike locations for 30 minutes on a 400X400 km grid with Norman, Oklahoma in the center (see domain b in figure 4.a.1).

2. Placement of the center of concentric circles. This can be done several ways. The first method used was manual location of the center of the ground strikes. This proved to be extremely subjective. The second method chosen was to average the locations of the strikes and use that as the center of the concentric circles. This allowed for all time blocks to be analysed *more* objectively than the manual method allowed. Centers were found for positive, negative and all cloud-to-ground strikes. However, upon analysis it was noticed that the center locations where not located within the heaviest concentrations of ground strikes. With the system analyzed, ground strikes were spread over an area 400 km long by 150 km wide (see figures 5.a.1-10). Questions were raised as to what fractal would be measured (i.e. convective area, stratiform area, etc.). To concentrate on the strongest convective areas, a last method was tried which worked extremely well. All results shown in Chapter V uses this centering technique. It involved constructing a 5x5 km grid over the analysis domain. The center of the grid block with

the highest concentration of negative ground strikes was used as the circle center. Due to the relatively small numbers of positive CGs, the -CG center was used for them as well.

3. Concentric circles are drawn around the center starting at a radius of one kilometer and moving outward in 1 km increments. The number of lightning strikes of each polarity located within each circle is determined (see figure 3.b.3).

4. A log/log plot of the cumulative number of strikes versus radius is generated (see figures 5.b.1-6 for a typical set of curves). The slope of this line is the fractal dimension (D). This step is subjective and some basic rules were followed to help minimize errors: a portion of the curve was chosen that was above N=10 and below where the curve becomes horizontal. With earlier centering techniques, two or three areas on the curve were used to determine a intermediate dimension, then these were averaged to obtain the overall fractal dimension. With the last method used, a single fractal dimension dominated most of the slope, so a single sample was adequate.

This concentric circle method was chosen over other methods of calculating fractal dimensions (e.g. box counting or area-perimeter methods. Barnsley, 1988: Lovejoy,

1982) for several reasons. It lends itself to automation very easily, it is mostly objective and, more importantly, it is a proven method that was used successfully to determine the fractal dimension of the universe (Takayasu, 1986). Plots of lightning ground-strike locations and the universe, as we see it, do look similar. Both appear to be an apparent random distribution of points (points of light for the universe).

Table 2. Fractal Dimensions		
Phenomena	Dimension	Researcher(s)
Cloud and rain patterns	1.35	Lovejoy, 1982
Coastline	1.2	Barnsley et al., 1988
Lightning	1.7	Niemeyer et al., 1984 *
Universe	1.2	Szalag and Schramm, 1895; Groth and Peebles, 1977 *
Craters on Moon	2.0	Mizutani, 1980 *
Asteroids	2.1	Mizutani, 1980 *
Meteorites	2.3	Mizutani, 1980 *
Collisions **	2.0	Mizutani, 1980 *
Earthquakes	1.3-2.06	Fujiwara et al., 1977 *
Catastrophe theory	1.7	Takayasu, 1986
* Reviewed in Takayasu, 1986 ** Bullet hitting rock		
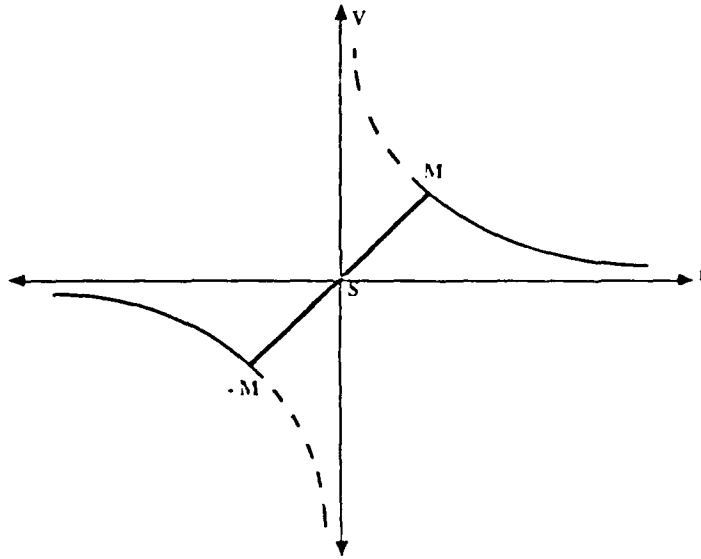
Figure 3.a.1: Theoretical (dashed line) and actual velocity distribution across a singularity (S). Maximum velocities are located at M and –M.
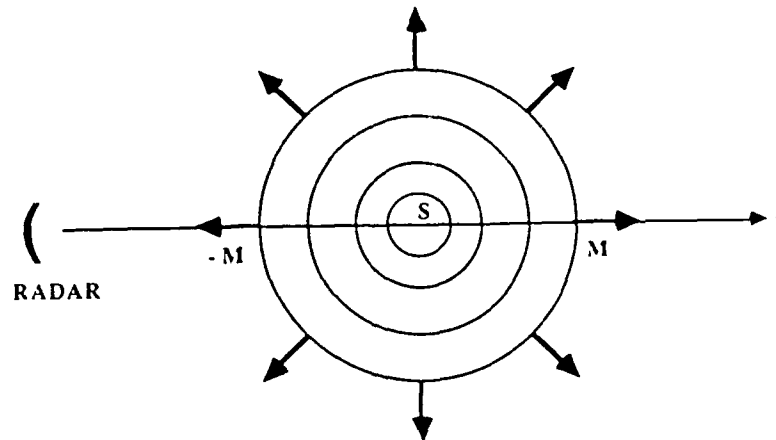
Figure 3.a.2: Local symmetry as it applies to a divergence (source) singularity. A convergence (sink) singularity is identical except the arrows are reversed (i.e. toward S).
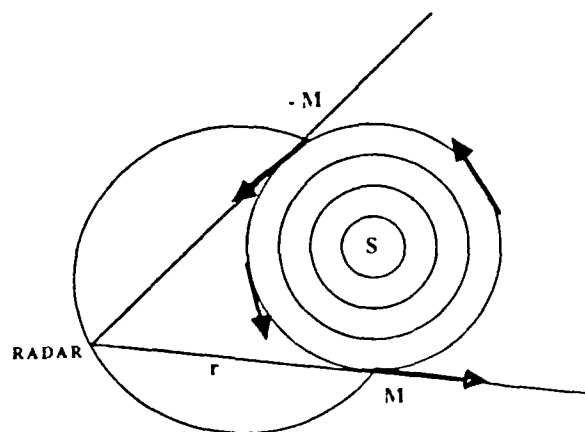
Figure 3.a.3:   Local symmetry as it applies to a cyclonic vort-
icity (rotation) singularity. An anticyclonic
vorticity singularity would rotate clockwise.
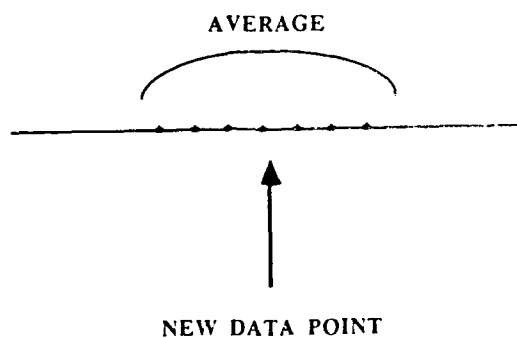
Figure 3.a.4:   Preprocessing doppler velocities involves
averaging seven gates to obtain one new data
point.
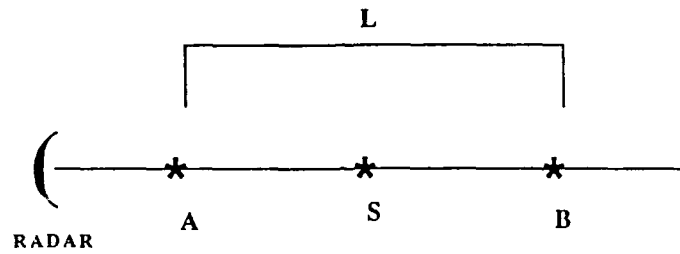
$$\text{DIVERGENCE SINGULARITY} = \frac{B - A}{L}$$

Figure 3.a.5: Divergence singularity calculation. A and B are velocities and L is distance.
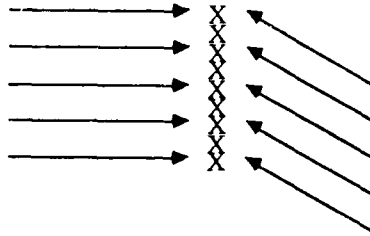
Figure 3.a.6: Example of convergence singularities. Divergence singularities have the arrows pointing in the opposite direction.
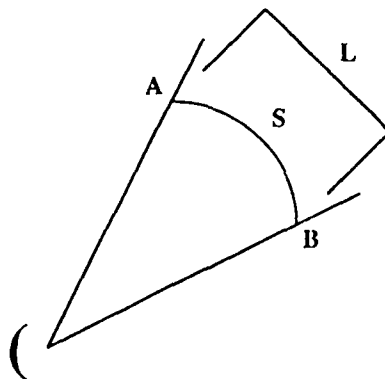
$$\text{VORTICITY SINGULARITY} = \frac{B - A}{L}$$

Figure 3.a.7: Vorticity singularity calculation. A and B are velocities and L is distance.
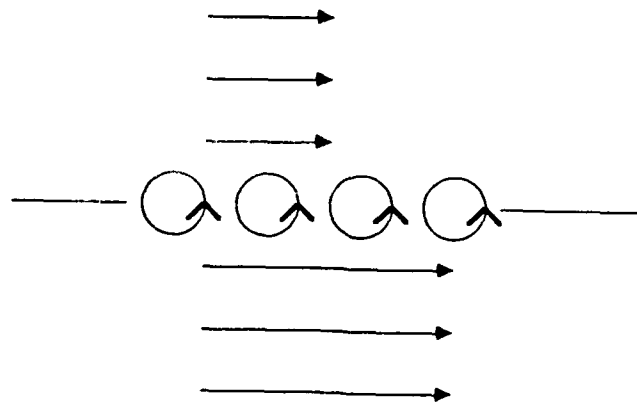
Figure 3.a.8: Example of cyclonic vorticity singularities. Anticyclonic vorticity singularities rotate clockwise.
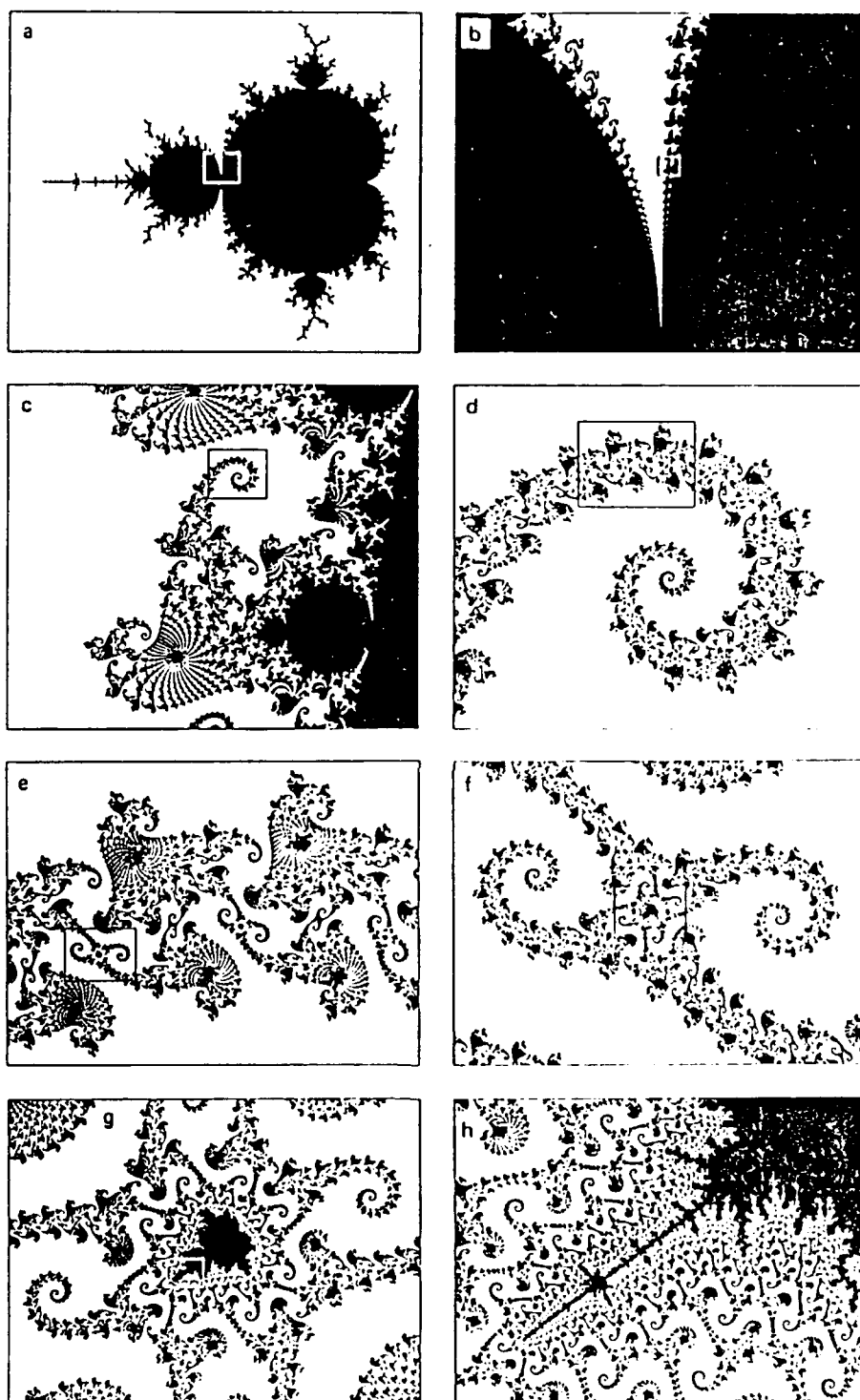
Figure 3.b.1: Example of a fractal (Mandlebrot set) magnified eight seperate times (adapted from Barnsley et al., 1988).

42

N PARTS SCALED BY RATIO R

1-DIMENSION

OR

$$N \frac{1}{R^1} = 1$$
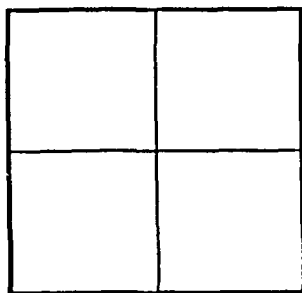
2-DIMENSIONS

$$N \frac{1}{R^2} = 1$$
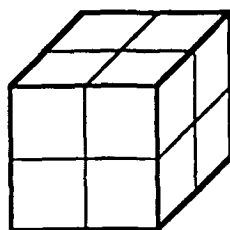
3-DIMENSIONS

$$N \frac{1}{R^3} = 1$$

IN GENERAL:
$$N \frac{1}{R^D} = 1$$

OR

$$LOG\ (N) = D\ LOG\ (R)$$

Figure 3.b.2: Derivation of fractal dimension (D) from tradi-
tional geometry (adapted from Bàrnsley et al.,
1988).

43
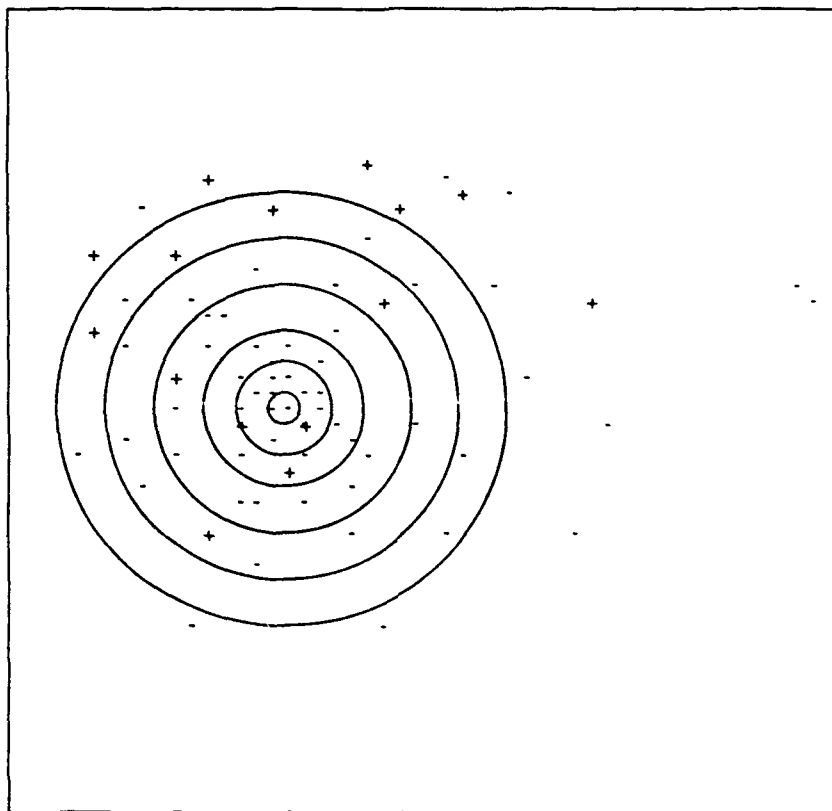
Figure 3.b.3:   Determining the fractal dimension of lightning
ground strikes (step 3).

CHAPTER IV

DATA AND DATA PROCESSING

A. Lightning Detection System

The lightning data used in this study is from the network operated by the National Severe Storms Laboratory (NSSL) in Norman, Oklahoma (Reap and MacGorman, 1989). This network is made up of four (4) wideband magnetic direction-finders in Oklahoma and three(3) in Kansas (see figure 4.a.1).

Each direction-finder consists of an antenna with two orthogonal loops and a flat plate electric field antenna (Rust and MacGorman, 1988). The two-loop antenna (one is orientated north/south and one east/west) is set to measure the peak magnetic field of a cloud-to-ground return stroke. This will usually occur when the lightning return stroke pulse is within 100 m of the ground (Krider et al., 1980). This assures that the part of the lightning channel being sampled is vertical or nearly so. Several criteria must be passed before a particular signal is accept-

ed in order to eliminate intracloud flashes. The voltages measured by the two loops give the direction of the lightning strike by: (MacGorman, 1989)

$$\theta = \tan^{-1} \frac{V_{EW}}{V_{NS}}$$

where θ is the direction of lightning strike, V_{EW} is voltage in the east/west loop and V_{NS} is voltage in the north/south loop. This, however, gives a 180° directional ambiguity since the sign of the current is not known a priori. The electric field antenna removes this ambiguity by measuring the charge lowered to ground and, therefore, eliminates one of the two possible directions given by the loop antenna. This also allows the system to measure both positive and negative cloud-to-ground flashes.

Data from these seven (7) direction-finders are sent to NSSL where they are archived onto magnetic tape. These data are also processed immediately by the position analyzer located at NSSL to give a "real-time" location of the lightning strike. This can then be easily displayed on a color monitor. This real-time location uses data from the two direction-finders closest to the strike. To reduce errors in strike location, the lightning data used in this study were optimized. The optimization process uses data from all direction-finders that observed the flash by using a chi squared technique to give a more exact location of the strike. After optimization, the

46

lightning data consists of the date (YYMMDD), julian date, time (HHMMSS.SSS i.e. to nearest millisecond), polarity of strike (positive means positive charge lowered to ground and negative means negative charge lowered), latitude and longitude of strike, number of strokes in the flash and relative amplitude for the first detected stroke of each strike.

The chi squared technique takes the general form: (MacGorman, 1989)

$$\chi^2 = \sum_i \frac{\left(\theta_{Mi} - \theta_{Si}\right)^2}{\sigma^2}$$

where x^2 is minimized, θ_{Mi} is the measured angle to strike from site i, θ_{Si} is the solution angle to strike from site i and σ is the typical error (approximately 1°). This reduces the location errors to within 10 km over all analysis area for this study and within 5 km for the portion of the domain where most of the activity is occurring (MacGorman, 1990).

Other errors include random error and site errors. Krider et al. (1976) estimated the random error in directions measured by each direction-finder to have a standard deviation of 1°-2° (also see Mach et al., 1986). Site errors are azimuthal errors (i.e. error in θ) due to surrounding buildings, terrain, power lines, etc. Mach et al. (1986) described how to determine the site error which can then be corrected automatically by the position ana-

lyzer. They also found that the detection efficiency, that is the fraction of all cloud-to-ground flashes that the network detects, is about 70% within 200-300 km of the center of the network (see dashed circles in figure 4.a.1). Reduced detection efficiency could be caused by delays in transmission time from one or more direction-finders.

Unfortunately, data on intracloud lightning from the NSSL's mobile lab (Rust, 1989) were not available for this case.

B. Doppler Radar

The Doppler radar data used in this study are from the Norman Doppler Radar operated by the National Severe Storms Laboratory (NSSL) in Norman, Oklahoma. The data were obtained from NSSL on four magnetic tapes in universal format (Barnes, 1980). Consecutive data from 2239Z on 27 May (1639 CST) to 0118Z on 28 May (1918 CST) was analyzed. To read the data, a library of Fortran routines called UFRDOP was also obtained from NSSL personnel.

Before applying the Doves analysis, the Doppler velocity data were preprocessed. As discussed in Chapter III, A, this included averaging seven (7) gates of data to get one (1) new data point with a length scale of approximately 1.5-2.0 km (see figure 3.a.4). At the same time, ve-

locities of 999.0 (i.e. missing data flag) and +/- 1.0 were removed. Also eliminated were velocities with corresponding spectrum width (spectrum width is a measure of the shear or turbulence within the resolution volume) of 15.0 m/s or greater (Doviak and Zrnic, 1984).

Table 3 documents the characteristics of the Norman Doppler radar. Figure 4.b.1 shows the altitude of the radar beam as a function of distance from the radar and elevation angle. It was derived using the 4/3rd earth model from Doviak and Zrnic (1984). This gives a quick way of estimating the altitude of singularity patterns found.

Table 3. Characteristics of the Norman Doppler Radar				
Time (CST)	16:39 to 17:20	17:20 to 17:58	17:58 to 18:39	18:39 to 19:17
Wavelength (cm)	10.52	10.52	10.52	10.52
Peak Power (kW)	499.39	499.39	499.39	499.39
Nyquist Velocity (m/s)	24.45	24.45*	34.23	34.24
Radar Constant	72.19	72.19	72.19	72.19
Gate Spacing (m)	210.0	210.0	150.0	150.0
Volume Depth (m)	150.0	150.0	150.0	150.0
Beam Width (deg)	0.81	0.81	0.81	0.81
Pulse Repetition (μs)	1075.0	1075.0	768.0	768.0
Pulse Duration (μs)	1.0	1.0	1.0	1.0
Antenna Gain (dB)	46.80	46.80	46.80	46.80
* Nyquist Velocity changes to 34.23 m/s after the start of this tape.				
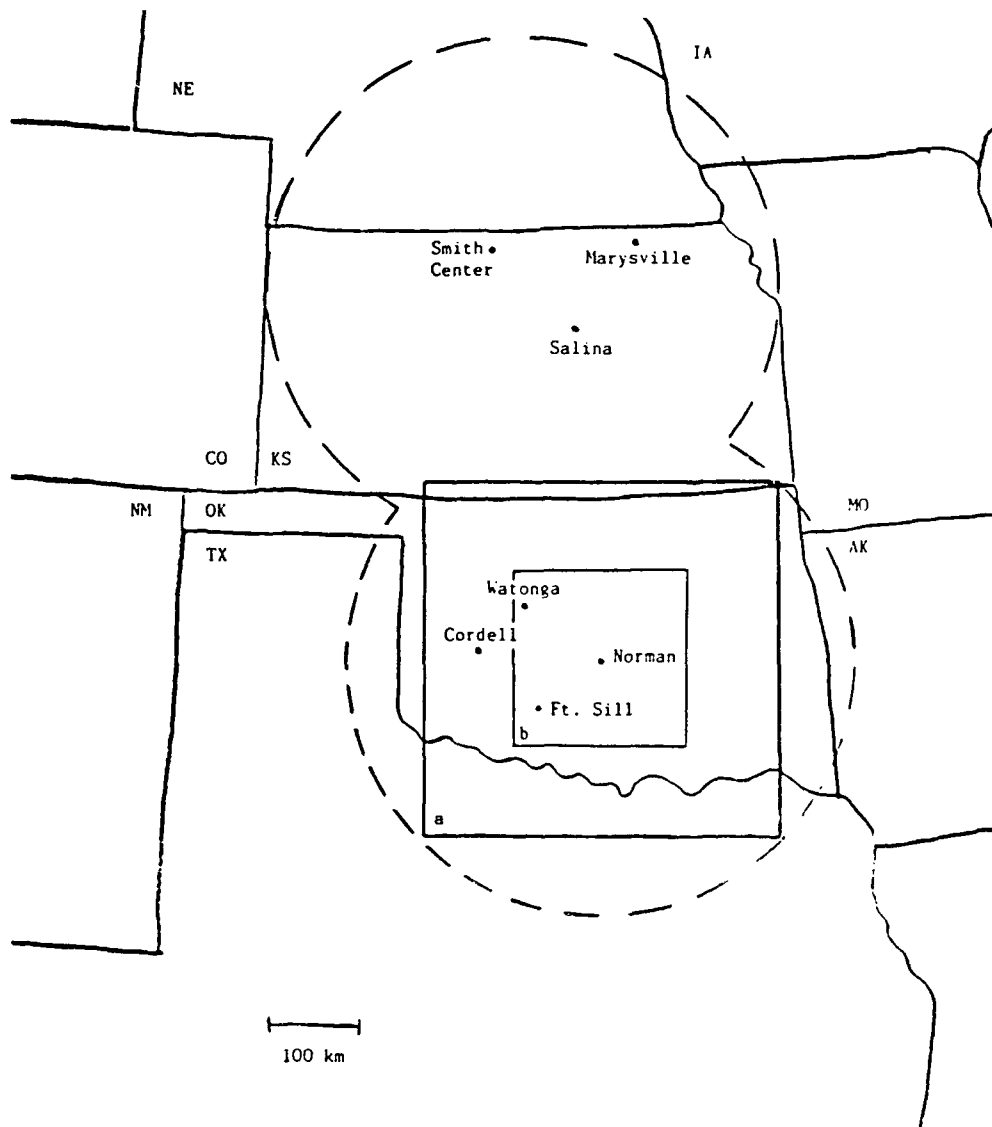
Figure 4.a.1:   The NSSL lightning detection network. Dashed
                lines are the approximate 70% detection effi-
                ciency. Larger square (a) is the fractal anal-
                ysis domain. The smaller square (b) is the sing-
                ularity analysis domain.
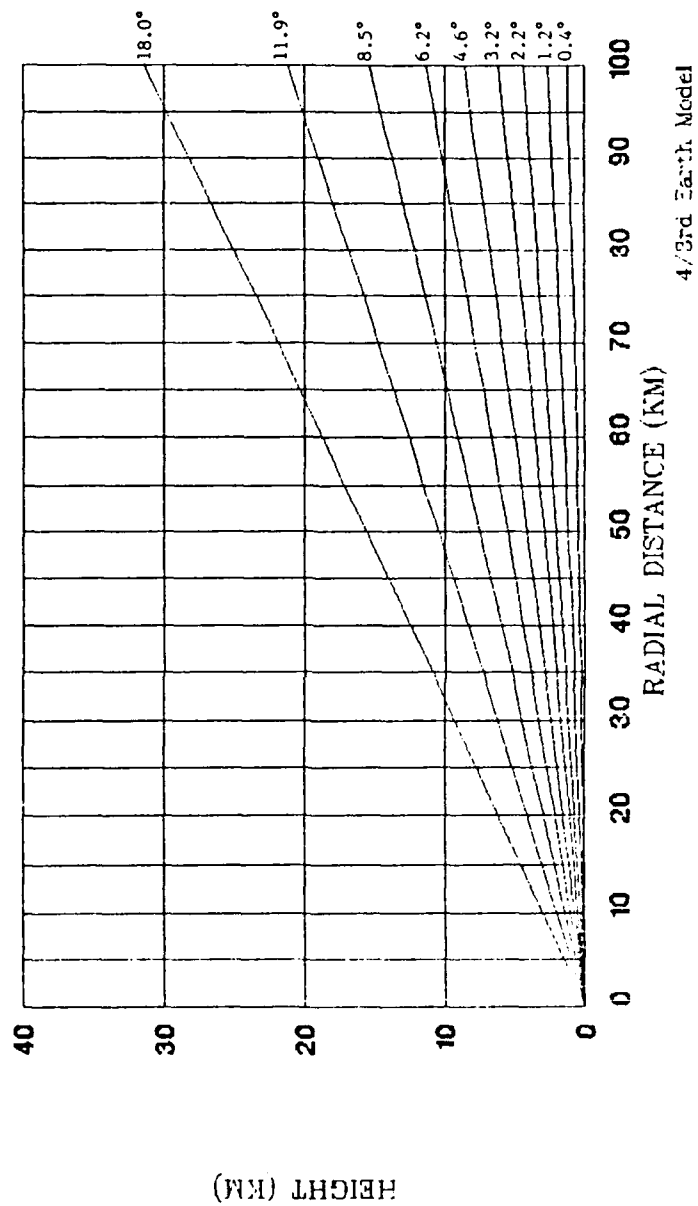
Figure 4.b.1: Altitude of radar beam with distance.

51

CHAPTER V

RESULTS AND DISCUSSION

A. Singularity Analysis

Figures 5.a.1-10 shows lightning data, in 30 minute blocks, for 2100Z-0200Z (1500-2000 CST) which is approximately one hour before and after the *DOVES* analysis. Note that most of the -CGs are in the southwest quadrant with several +CGs downwind (i.e. northeast) of the -CG region. This is similar to the bipole pattern discussed by Orville et al. (1988). However, in this storm system, several +CGs are located within the main core region (i.e. mixed in with the -CGs). This makes finding a +CG center very difficult (as was found in the fractal analysis) and determining the bipole distance impossible. The right side of the lightning plots are the lightning statistics. **TOTAL #** is the total number of lightning ground strikes within the 400X400 km grid. **# POS** and **# NEG** are the numbers of positive and negative cloud-to-ground lightning within the MCC only (i.e. lightning more than 110 km east

of Norman is excluded).

Note: The figures presented in this thesis lose much of their impact because they are in black and white. This is especially true with the singularity displays where color can give both the sense of the singularity (e.g. divergent or convergent) and the order of magnitude of the singularity. Most of this is lost in the black and white renditions. For this, I apologize.

The most significant and encouraging result of the singularity analysis is the correlation between background convergence values calculated by *DCVES* and the number of negative ground strikes (see figure 5.a.11a). The results for all CG flashes (not shown) are the same as for -CG flashes. Approximately 10 minutes after a maximum in background convergence, at the lowest elevation angle (i.e. 0.4°), there is a corresponding peak in the number of negative ground strikes (5 minute average). Likewise, approximately 10 minutes after a minimum in background convergence (at 2343Z (1743 CST) the value goes to divergence) there is a corresponding minimum in the flash rate. In other words, there is a maximum in background convergence shortly before the peak in CG flash rates. During the peak flash rates, the background convergence goes to divergence as the gust front spreads out ahead of the convective line. Immediately after this, the flash rate drops from nearly 200 in a five minute average to around

53

115. The background convergence values calculated by *DOVES* are on the order of 10^{-5} s^{-1}, which is in good agreement with values found by Newman (1971) during severe storms. Positive cloud-to-ground lightning shows less correlation than -CGs to background convergence (see figure 5.a.11b). The time lag between a peak in background convergence and +CG flash rates varies between 10-25 minutes. The +CG flash rate does, however, decrease at the time of background divergence and maximum gust front outflow just as the -CG flash rate did. Unfortunately, Doppler radar data were not available for the time periods of the secondary peak in -CG flash rates (at the end of the analysis period) and the overall peak in +CG flash rate (earlier in the analysis period).

Similar findings were discussed by Williams et al. (1989). They analyzed all lightning (i.e. CG and IC) for several microburst producing storms in Alabama. They found that the peak lightning flash rate (which was dominated by IC) occurred 5-10 minutes prior to the maximum outflow velocities at the surface. This is strikingly similar to our finding with low level background divergence calculated by *DOVES*. The peak in CG flash rates also lagged the peak in total lightning by 5-10 minutes (Williams et al., 1989) and were, therefore, coincident with the strongest outflow. In this study, the singularity analysis places the strongest outflow of the gust front

(which will be discussed in more detail shortly) within two (2) minutes of the peak CG flash rate. Williams et al. (1989) attribute the increase in CG flash rates to descending ice particles within the storms. The descending ice particles accelerate the downdraft by inducing negative buoyancy and produce the downburst/microburst.

Low-level moisture convergence has also been shown by Reap and MacGorman (1989) to be one of the best predictors of the *probability* of ground strikes of both polarities. For -CGs, low-level moisture convergence was the best predictor of the 31 model fields they analyzed. Whereas for +CGs, moisture convergence placed fifth. This supports the results of the singularity analysis.

Folded velocities are discussed further in Chapter VI. However, one point of discussion pertaining to lightning is in order here. *DOVES* is capable of locating any significant shear zone within the scan, either real or due to velocity folding. At 8.5° elevation, an area of folded velocities (i.e. jet maximum - the nyquist velocity is 34.23 m/s) at an altitude of approximately 10 km (see figure 4.b.1) is located immediately east, or east-northeast, of the core lightning area (i.e. the core of the MCC) from approximately 2330Z-0010Z (1730-1810 CST) (see figures 5.a.12-16). I speculate that this feature is the lower portion of a jet streak bypassing, or side stepping the MCC core. As time progresses, the singularities weak-

en and move slowly eastward. This supports the low level convergence findings discussed above and suggests that the jet streak is enhancing the storm-top outflow, allowing stronger vertical motion within the MCC and possibly enhancing charge generation. Radar data prior to 2330Z (1730 CST) for this elevation has a nyquist velocity of 24.45 m/s and, therefore, shows a broad area of folded velocities and not only the jet core at that altitude.

A note on the singularity display (i.e. figures 5.a.12-22 and 6.1-2) is now in order. Across the top of the display is the radar location, date, time (CST) elevation angle, sweep number and the threshold of the type of singularities plotted. A threshold of 0.009 means that all singularities larger than +/- 0.009 s^{-1} are plotted. On the right hand side are the legends for singularities and lightning, total number of CGs plotted, bracket time and flash rate (flashes/minute). For divergence singularity display, D represents positive divergence singularity and C negative (or convergence). Likewise, C and A are used for cyclonic and anticyclonic for the vorticity singularity display. Again, colors transfer much more information to the user. The bracket time is the time on each side of the radar data that lightning data is plotted. Across the bottom of the display is the background diver-

gence (0.4˚ only) and the percentage of the ground strikes that were positive. Within the display are weather reporting stations with Norman (OUN) in the center.

Another significant feature located by the *DOVES* analysis (as mentioned above) is a gust front. The gust front was first located at an elevation angle of 2.2˚ at 2325Z (1725 CST) (see figure 5.a.17). It was not observed, by radar, at the surface until 2333Z (1733 CST) and then was very weak (see figure 5.a.18). This gives a conservative lead-time estimate of 5-8 minutes, possibly more. The exact lead-time possible can not be determined in general because it can depend on the scanning rate of the radar. The gust front reached maximum strength, as observed by *DOVES*, at the surface at 2343Z (1743 CST) near the time of maximum ground strikes (see figure 5.a.19).

As the gust front progresses eastward, new convection, and associated ground strikes, develops on the northern end of the outflow. This could have been anticipated by looking at the *DOVES* plot (see figure 5.a.20). Clearly the northern portion of the gust front has the strongest convergence and would favor new convection. This is also the region where the mesocyclone develops.

At 2337Z (1737 CST), a small area of positive vorticity singularities is first observed in the northern portion of the gust front (see figure 5.a.21). At this time, there has been a substantial increase in -CGs along, and

behind, the outflow boundary over the last 12 minutes (compare to figure 5.a.17). By 0004Z (1804 CST) this region has strengthened into a well defined mesocyclone on the traditional Doppler velocity display and is well defined on the *DOVES* plot (see figure 5.a.22). Again, a significant lead-time is given by the *DOVES* analysis scheme. In this case, the conservative lead-time is approximately 20 minutes or more.

B. Fractal Analysis

According to fractal theory, we should see a straight line on a log/log plot which gives the fractal dimension (the slope is the dimension. See Chapter III, B.). Figures 5.b.1-2 show typical plots of total and negative cloud-to-ground lightning strikes versus radius from center (see figures 5.a.1-10 for actual lightning diagrams). We notice that the plots of negative CG strikes are nearly identical to those of all CG strikes. Immediately we see that both plots show the presence of a fractal! And this is persistent throughout the entire five hour analysis. Table 4 lists average fractal dimensions calculated for all CGs, -CGs and +CGs for various distances from the center.

Note: If a fractal dimension is calculated for a segment of a plot, the dimension retains information on the number of strikes closer to the center location, but no

58

information on strikes farther out is included. For exam-
ple: If you calculate the dimension (remember the slope of
the line is the dimension) for a segment from 50 to 100
km, the dimension will have information on, or more pre-
cisely is measuring the fractal from, lightning strikes
from the center to 100 km. Therefore, the fractal dimen-
sion for the segment 100-200 km should not be interpreted
as a measure of the fractal 100-200 km from the center.
In other words, the core of the lightning activity scales
the dimension of the rest of the lightning activity.

Looking at the plots for positive ground strikes (see
figures 5.b.3-4) we see that the presence of a fractal is
not clear. Some segments do appear to be linear but we
are hampered by the low total number of +CGs in each 30
minute block (which ranges from 43-140 strikes). The
fractal dimensions given in table 4 are not given with any
confidence and should be treated as uncertain. To bypass
this problem of sample size, a single fractal analysis for
the entire five hour period was conducted. A smoother
curve is obtained (see figure 5.b.5) but it is still not
linear. A slow curve is seen from 20 km to the domain
edge. A small segment, 10-20 km, is linear but we still
have only 40 out of 801 total strikes included (compare to
figure 5.b.6). Part of the difficulty may be due to using
the -CGs strike locations to calculate a fractal for +CGs.
The -CG strike maximum was chosen because it is the center

59

of the strongest convection. If +CGs are truly a more stratiform phenomena, we would not expect a fractal to emerge. Also, using a five hour time period may distort the target fractal (time is a dimension too). In any case, for +CGs, no *apparent* fractal exists for this storm for the time period analyzed in this manner.

As can be seen from Table 4, the fractal dimension for negative and total ground strikes is 1.2, slightly smaller than the number Lovejoy (1982) gave for cloud and rain areas using an area-perimeter method (1.35) and is the same as the dimension found for coastlines and the universe (see Table 2). Note also that the dimension decreases as a larger area is analyzed. The dimension goes to one, that is linear (note the linear appearance in the strikes shown in figures 5.a.1-10). It is interesting to note that for the single five hour analysis, both all and -CGs have a higher fractal dimension, 1.7, which is the **same as the dimension of lightning channels** and for catastrophe theory. No conclusions are drawn from this similarity at this time. The 1.7 dimension is also near the dimension of 2.0 given in Table 2 for a bullet hitting stone and within the range found for earthquakes.

The fractal dimensions obtained from both 30 minute and five hour time periods for +CGs do not show signs of

fractals being present while for -CGs a fractal is apparent. That may mean that self-similarity is *not* a inherent property of +CGs but is for -CGs.

Figure 5.b.7 shows the number of lightning strikes within 5 km of the center versus fractal dimension. It shows that as the number of strikes in close to the center increases, the dimension (calculated from near the center out to 100 km) decreases. This pattern is seen, but not as strongly, in the dimension calculated from near the center to 20 km (see figure 5.b.8). This could be due to geometric considerations (large number of strikes near the center may remove available charge from other areas farther out causing a linear appearance) or strike distribution considerations (number of strikes near the center scaling the rest of the lightning) or both. Which is true was not determined from this type of analysis. A new, hybrid technique is needed to distinguish between geometric and distribution effects.

In summary, fractals appear to be present in the -CG (and therefore all CG) data but not +CG strikes. The fractal dimension for all and -CG strikes for one, five hour analysis period is the same as was found earlier for lightning channels. A strong correlation is found between the number of strikes close to the center and the fractal dimension out to 100 km. Additional research is needed to

answer some basic questions. These include: 1) What is the fractal being measured?, 2) Why is no strong fractal seen in the +CG data? and 3) What is the best method of calculating the fractal dimension that will lead to meaningful conclusions from the results?

Table 4 Fractal Dimensions of Lightning Ground Strikes			
Segment (km)	All CGs	-CGs	+CGs
Near center to 20 *	1.24	1.21	NA
Near center to 100	1.03	1.01	NA
2-20 (5 hr block)	1.72	1.70	NA
10-20 (5 hr block)	NA	NA	3.87
10-100 (5 hr block)	NA	NA	1.80
60-170 (5 hr block)	NA	NA	0.89
* Near center varies from 2 to 7 km. Unless noted all averages are from 30 minute block analysis.			

C. Future Work

Much additional work must be done to explore fully both techniques outlined here. The *DOVES* analysis shows

great promise as a combined algorithm for locating torna-
does, microbursts, gust fronts, mesocyclones and areas of
folded velocities and for calculating background diver-
gence. Numerous case studies must be done before it can
be put into an operational setting, such as NEXRAD. The
gust front shown here was oriented perpendicular to the
radar beam. What would happen if the convergence line was
oriented along the beam? Seven gates were averaged in
this analysis. Should this be different for different
situations or locations? More work with *DOVES* derived
background convergence must also be done, in particular,
calculating background convergence in specific portion of
a storm system. Case studies on other storm types is also
warranted. This is an interesting portion of the analysis
and could be very useful to the meteorological community
upon maturity. It may even lead to an additional mi-
croburst precursor.

This study has only scratched the surface of fractal
analysis and lightning. Many more storms and storm types
must be analyzed. Better, more sophisticated centering
techniques (such as using peak reflectivity areas) should
be developed along with a set of guidelines as to where on
the log/log plot to take the slope. A start at some basic
rules was attempted here and must be matured (see Chapter
III, B). Comparison to other techniques of determining
the dimension, such as the area-perimeter method, would be

helpful in determining whether or not +CGs have an associated fractal. One technique may solve the question of whether the correlation shown in figure 5.b.7 is geometric or distribution in nature. It would involve gridding the lightning data, sorting the grid by the number of strikes within each grid square, then summing over the area of the grid squares (starting at the grid box with the most strikes and ending when you reach the box that first goes to zero). If the relationship noted above is distribution dependent, then this type of analysis should yield a fractal looking plot.

Comparison of fractal dimensions from storms in the Midwest, east coast, Japan and other locations around the world would help determine if there is a geographic or seasonal variations in the existence of +CG fractals as there are in percentages of positive strikes.

Fractal geometry is less than 20 years old. It will take decades, or even centuries, to explore fully this new branch of mathematics. It may also take that long to understand fully the nature of lightning!
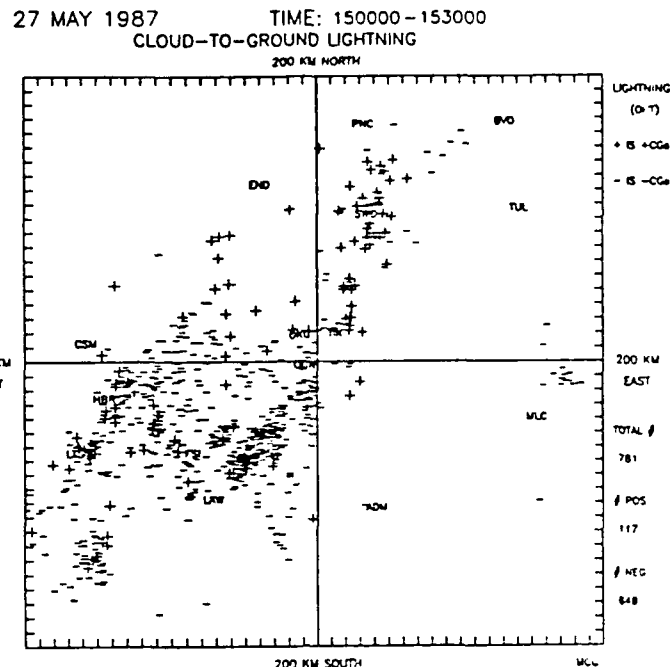
Figure 5.a.1: Cloud-to-ground lightning activity for 2100–2130Z (1500–1530 CST) on 27 May, 1987. Positive ground strikes are depicted as +, negative ground strikes as –. The number of strikes are listed on the right side of the plot.
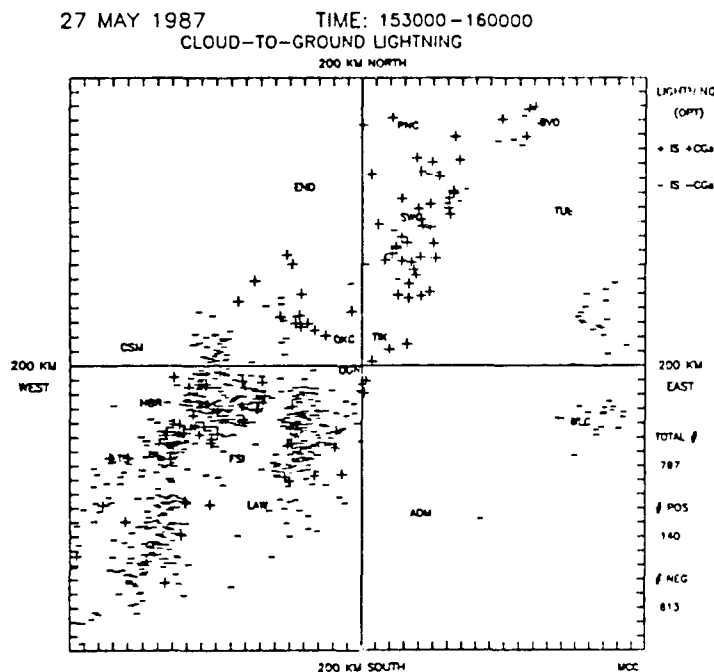

Figure 5.a.2: Same as Figure 5.a.1 except for 2130–2200Z (1530–1600 CST).

65

27 MAY 1987   TIME: 160000–163000
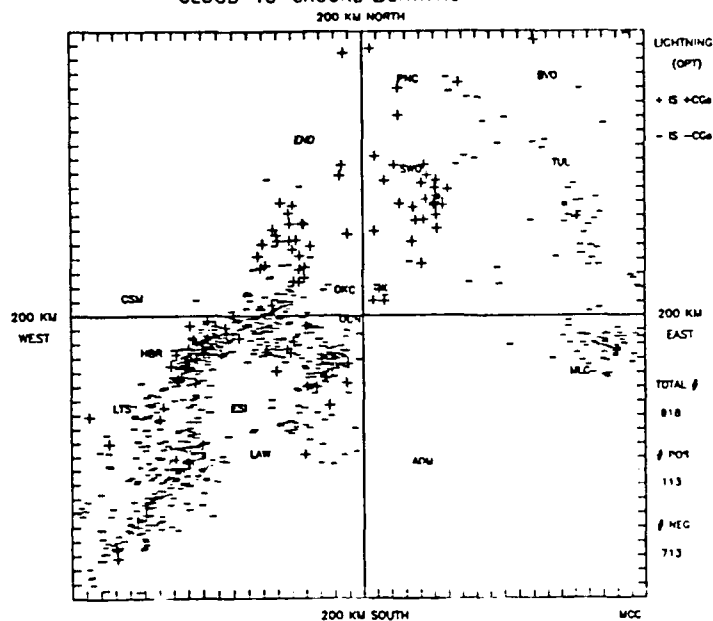CLOUD-TO-GROUND LIGHTNING

Figure 5.a.3:   Same as figure 5.a.1 except for 2200–2230Z
(1600–1630 CST).

27 MAY 1987   TIME: 163000–170000
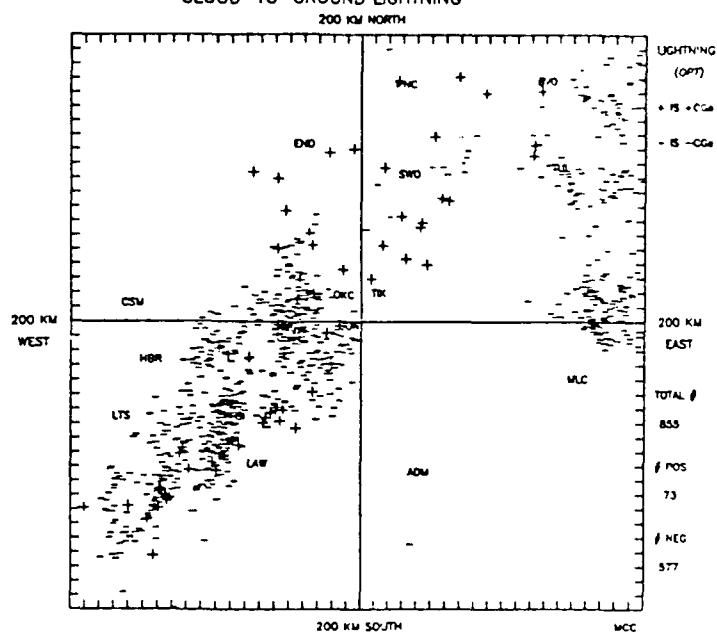CLOUD-TO-GROUND LIGHTNING

Figure 5.a.4:   Same as Figure 5.a.1 except for 2230–2300Z
(1630–1700 CST).

66

27 MAY 1987   TIME: 170000-173000
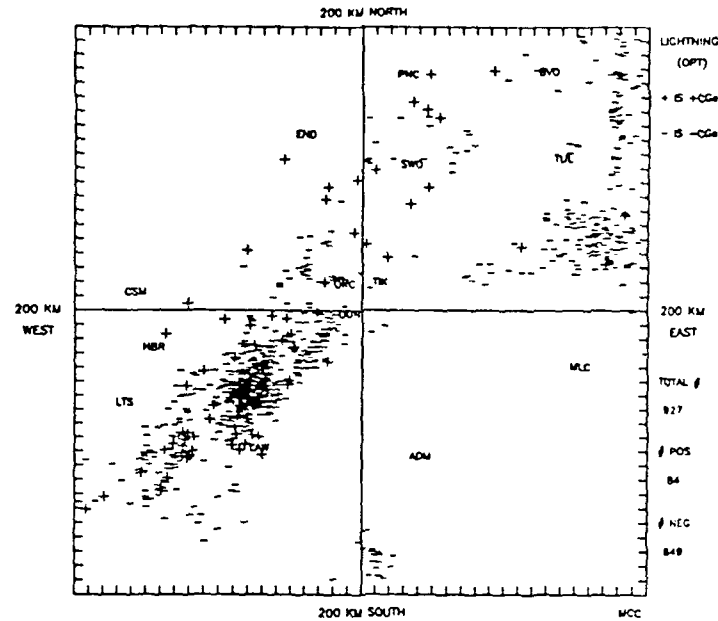CLOUD-TO-GROUND LIGHTNING

Figure 5.a.5:   Same as Figure 5.a.1 except for 2300-2330Z
(1700-1730 CST).

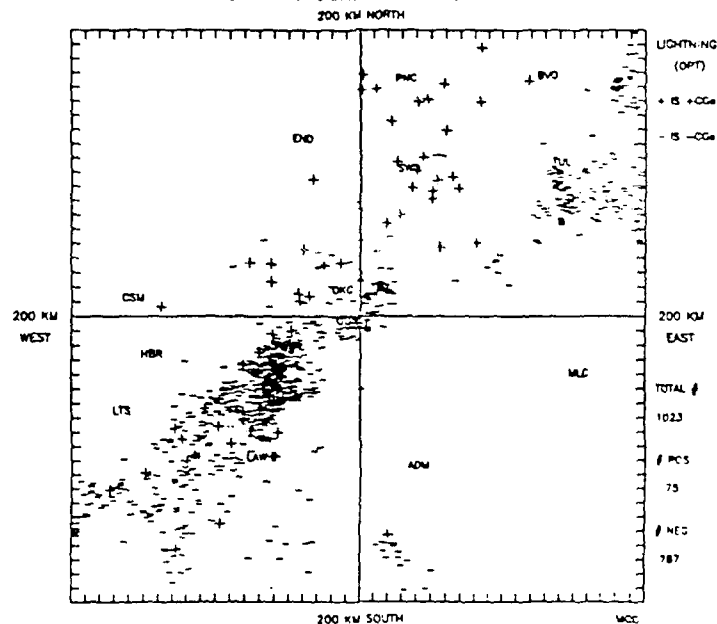27 MAY 1987   TIME: 173000-180000
CLOUD-TO-GROUND LIGHTNING

Figure 5.a.6:   Same as Figure 5.a.1 except for 2330-0000Z
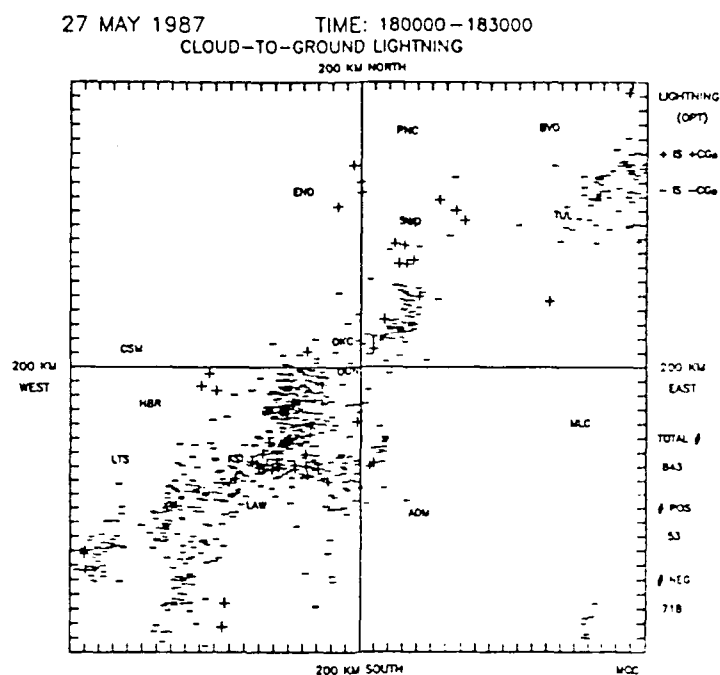(1730-1800 CST).

Figure 5.a.7: Same as Figure 5.a.1 except for 0000-0030Z on 28 May, 1987 (1800-1830 CST on 27 May).
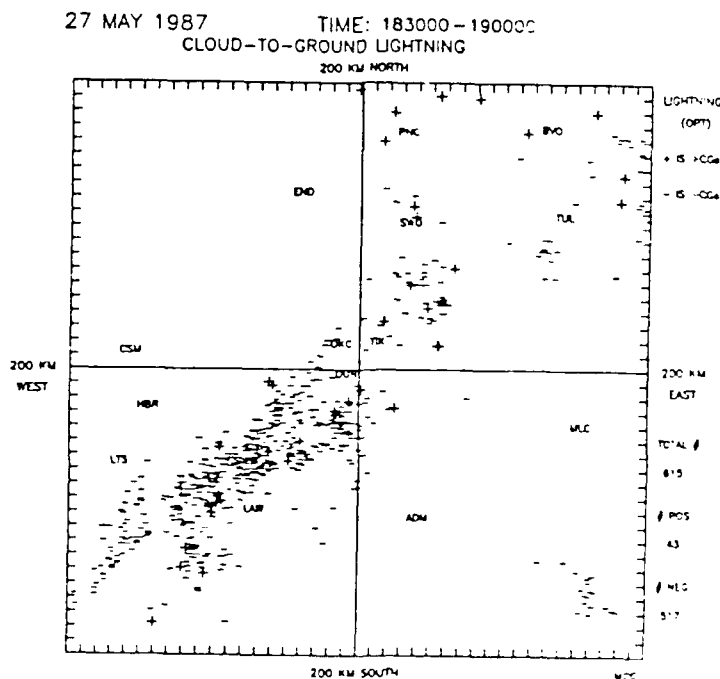
Figure 5.a.8: Same as Figure 5.a.1 except for 0030-0100Z on 28 May, 1987 (1830-1900 CST on 27 May).

27 MAY 1987　　　　TIME: 190000-193000
CLOUD-TO-GROUND LIGHTNING
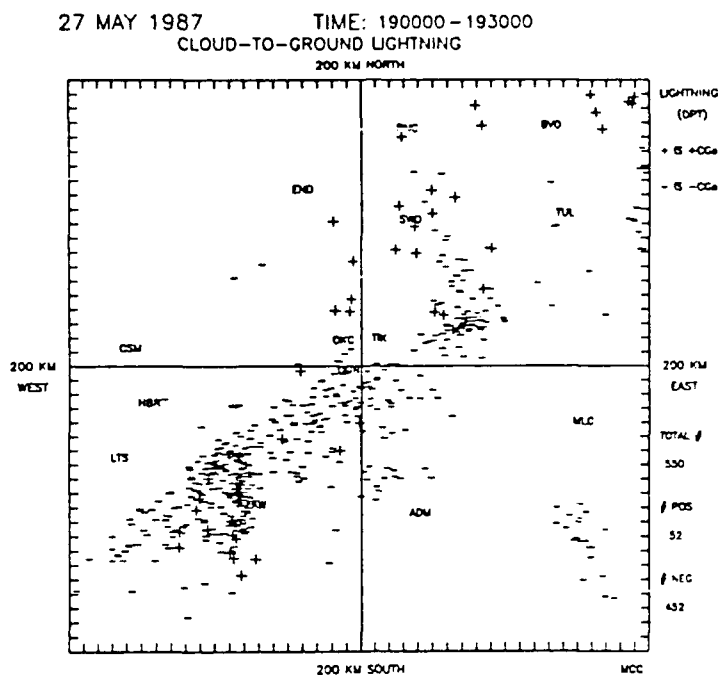
Figure 5.a.9:　Same as Figure 5.a.1 except for 0100-0130Z on
28 May, 1987 (1900-1930 CST on 27 May).

27 MAY 1987　　　　TIME: 193000-200000
CLOUD-TO-GROUND LIGHTNING
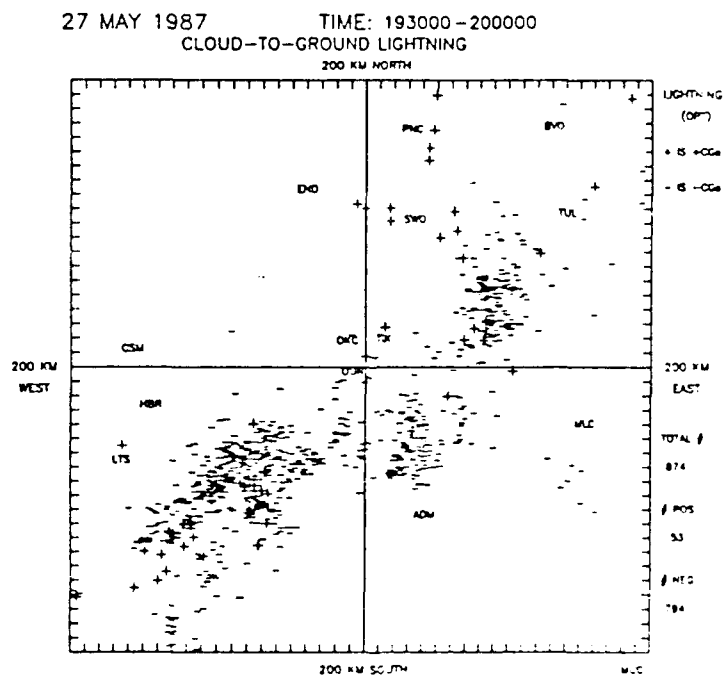
Figure 5.a.10:　Same as Figure 5.a.1 except for 0130-0200Z on
28 May, 1987 (1930-2000 CST on 27 May).
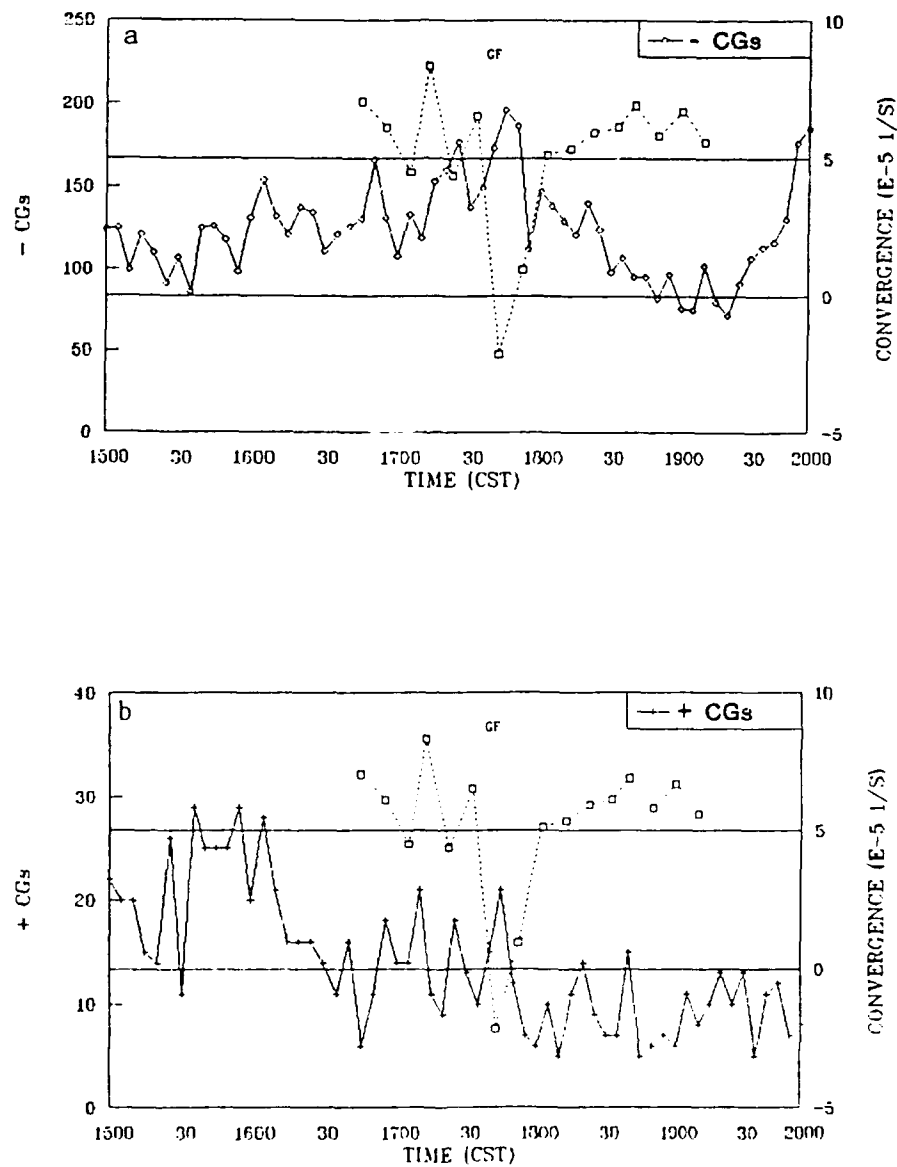
Figure 5.a.11: Negative (a) and positive (b) cloud-to-ground lightning (solid line) and background divergence calculated by singularity analysis (dashed line) plotted versus time. GF is the approximate time of maximum gust front outflow.

NORMAN   RADAR   DATE: 52787   TIME: 172923–173021   CS
ELE (deg):   8.5   SWEEP NUMBER   3   THRESHOLD   DIV   0.0125

100 KM NORTH

D IS DIV

C IS CONV

LIGHTNING
(OPT)

+ IS +CGs

– IS –CGs

OKC   TIK

100 KM
WEST

OUN

100 KM
EAST

229 CGs

BRACKET:

5 MINS

STRIKE
RATE:
(PER MIN)

20 88

FSI

LAW

100 KM SOUTH   3.930   % POSITIVE
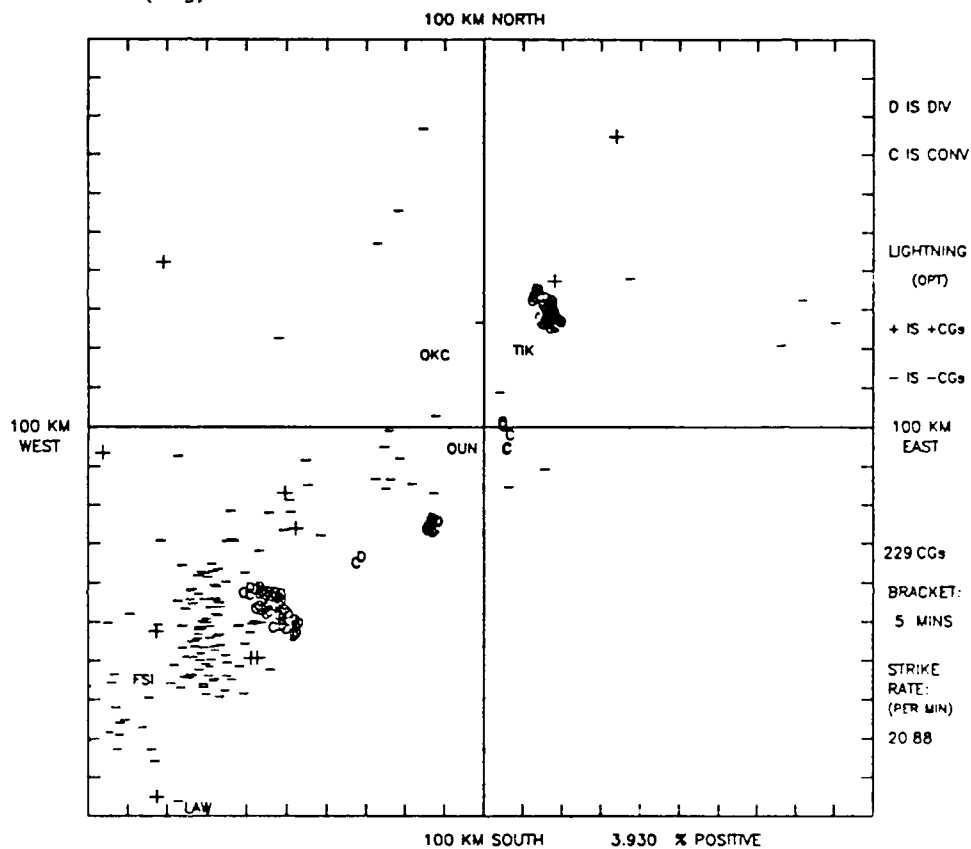
Figure 5.a.12:   Divergence Singularity display for 2329Z (1729 CST)
on 27 May, 1987.

71

NORMAN RADAR DATE: 52787 TIME: 173905-174003 CS
ELE (deg): 8.5 SWEEP NUMBER 5 THRESHOLD DIV 0.0100

Figure 5.a.13: Same as Figure 5.a.12 except for 2339Z (1739CST).

NORMAN RADAR DATE: 52787 TIME: 174848-174946 CS
ELE (deg): 8.6 SWEEP NUMBER 7 THRESHOLD DIV 0.0100
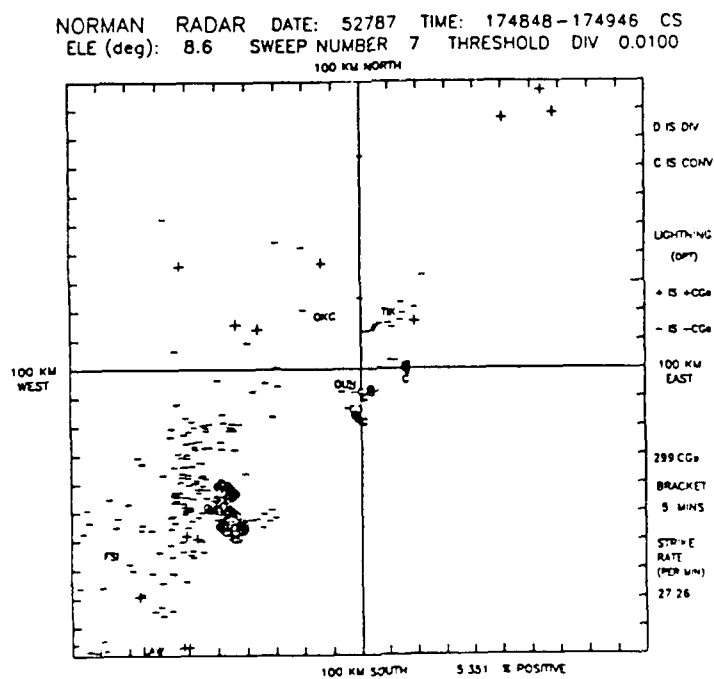
Figure 5.a.14: Same as Figure 5.a.12 except for 2349Z (1749 CST).

72

NORMAN RADAR DATE: 52787 TIME: 180814–180912 CS
ELE (deg): 8.5 SWEEP NUMBER 3 THRESHOLD DIV 0.0090

Figure 5.a.15: Same as Figure 5.a.12 except for 0008Z (1808 CST)
on 28 May, 1987.

NORMAN RADAR DATE: 52787 TIME: 181756–181855 CS
ELE (deg): 8.5 SWEEP NUMBER 5 THRESHOLD DIV 0.0090
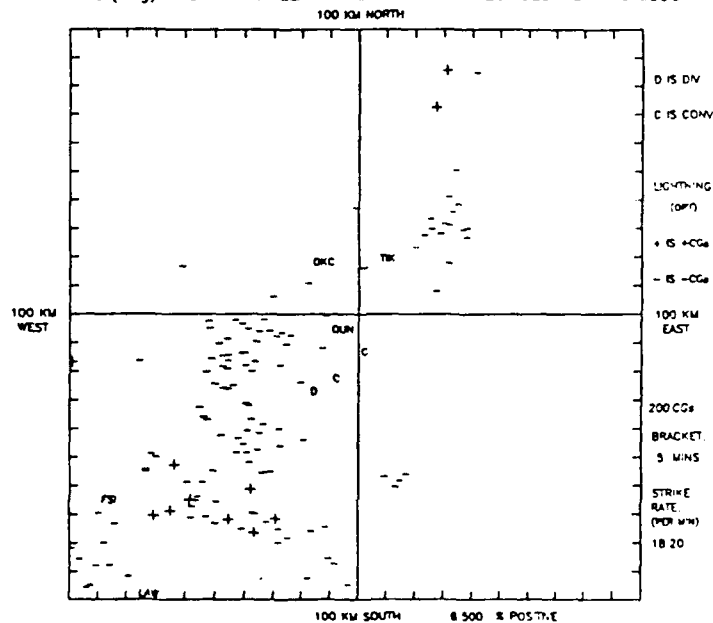
Figure 5.a.16: Same as Figure 5.a.12 except for 0018Z (1818 CST)
on 28 May, 1987.

73

NORMAN   RADAR   DATE: 52787   TIME: 172517—172615   CS
ELE (deg):   2.2   SWEEP NUMBER   3   THRESHOLD   DIV   0.0075

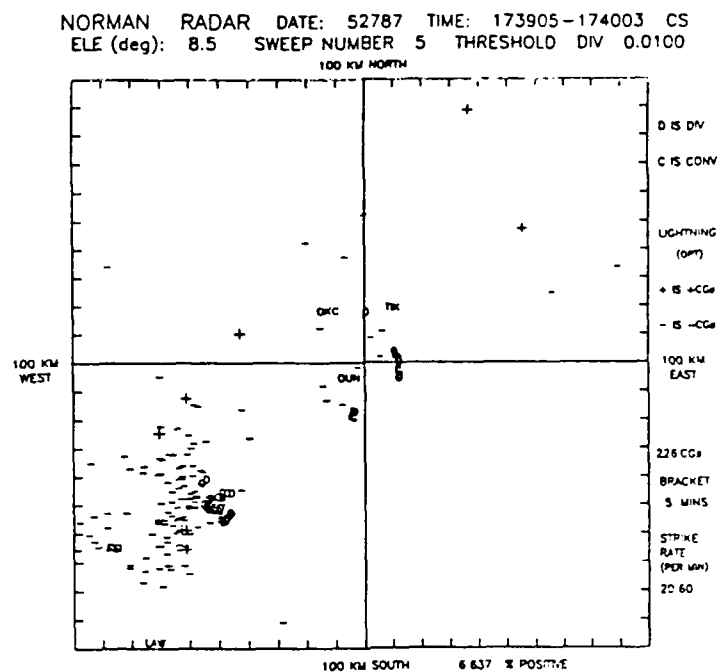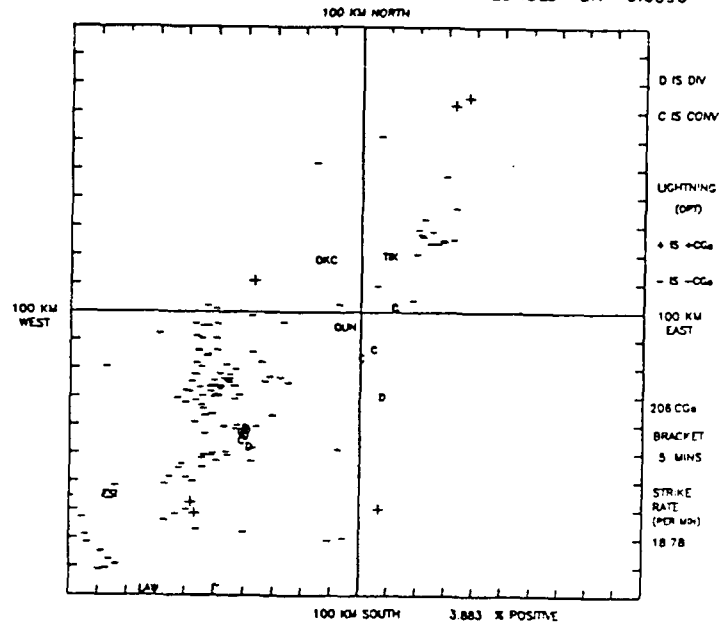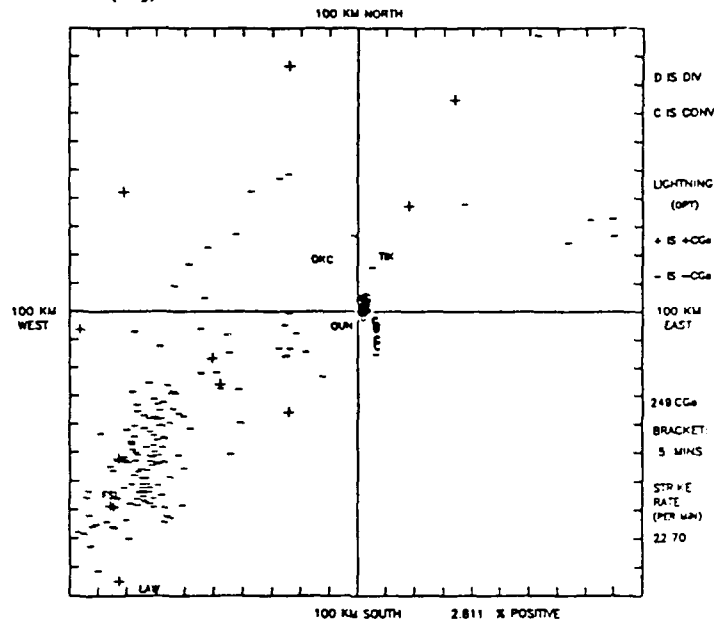Figure 5.a.17:   Divergence singularity display for 2325Z (1725 CST)
on 27 May, 1987.   Elevation angle is 2.2°.
Note gust front east and southeast of Norman (OUN).

NORMAN   RADAR   DATE: 52787   TIME: 173256—173354   CS
ELE (deg):   0.4   SWEEP NUMBER   3   THRESHOLD   DIV   0.0075
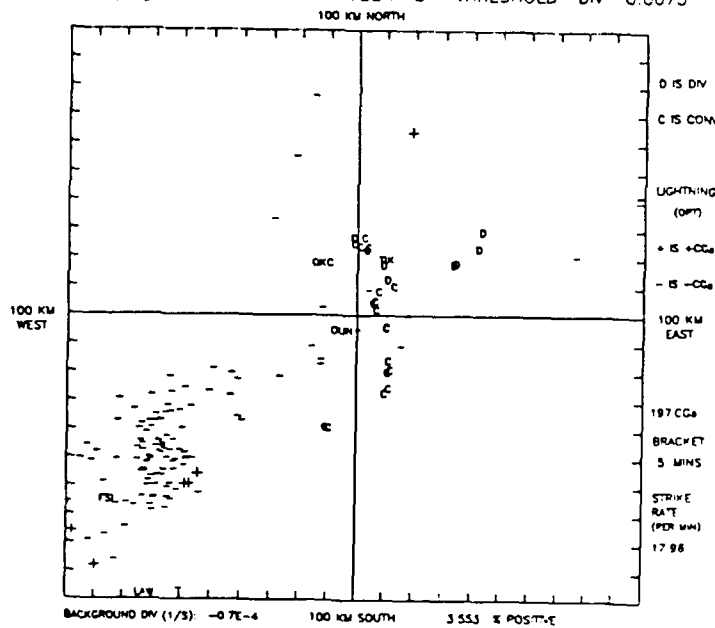
Figure 5.a.18   Same as Figure 5.a.17 except for 2333Z (1733 CST)
and elevation angle is 0.4°.

74

NORMAN RADAR DATE: 52787 TIME: 174239-174337 CS
ELE (deg): 0.4 SWEEP NUMBER 5 THRESHOLD DIV 0.0085
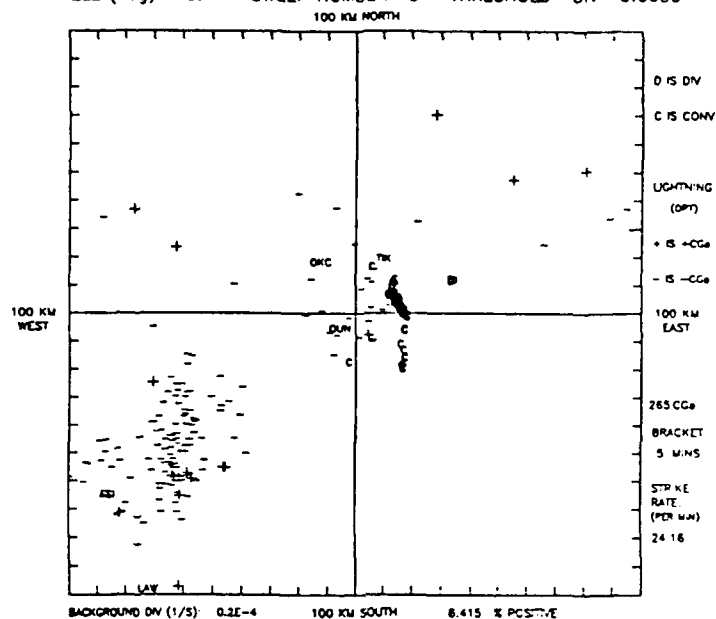
Figure 5.a.19: Same as Figure 5.a.18 except for 2343Z (1743 CST).
Gust front at maximum outflow strength.

NORMAN RADAR DATE: 52787 TIME: 180205-180303 CS
ELE (deg): 0.4 SWEEP NUMBER 1 THRESHOLD DIV 0.0080
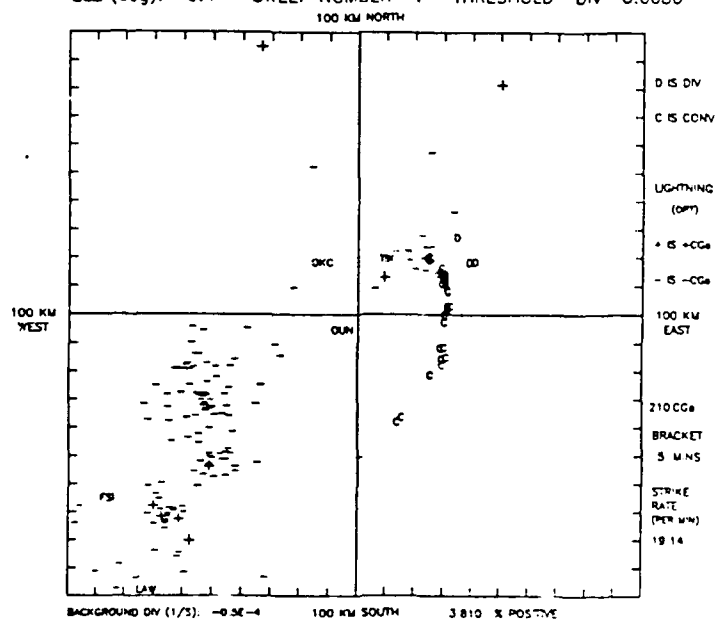
Figure 5.a.20: Same as Figure 5.a.18 except for 0002Z (1802 CST)
on 28 May, 1987. Note increased lightning
activity on northern end of gust front.

75

NORMAN   RADAR   DATE: 52787   TIME: 173702–173800   CS
ELE (deg): 4.6   SWEEP NUMBER 5   THRESHOLD VORT 0.0090
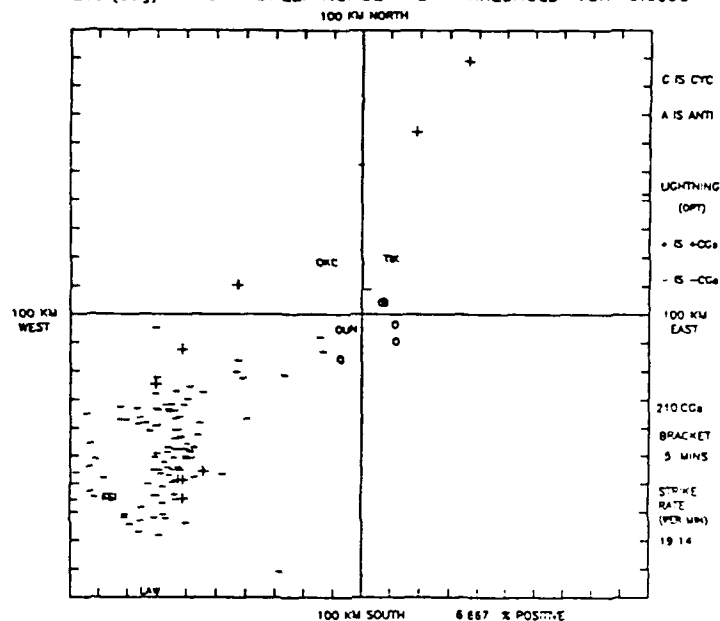
Figure 5.a.21:   Vorticity singularity display for 2337Z (1737 CST)
on 27 May, 1987. Note rotation on northern end
of gust front (compare Figure 5.a.19).

NORMAN   RADAR   DATE: 52787   TIME: 180408–180506   CS
ELE (deg): 2.3   SWEEP NUMBER 3   THRESHOLD VORT 0.0080
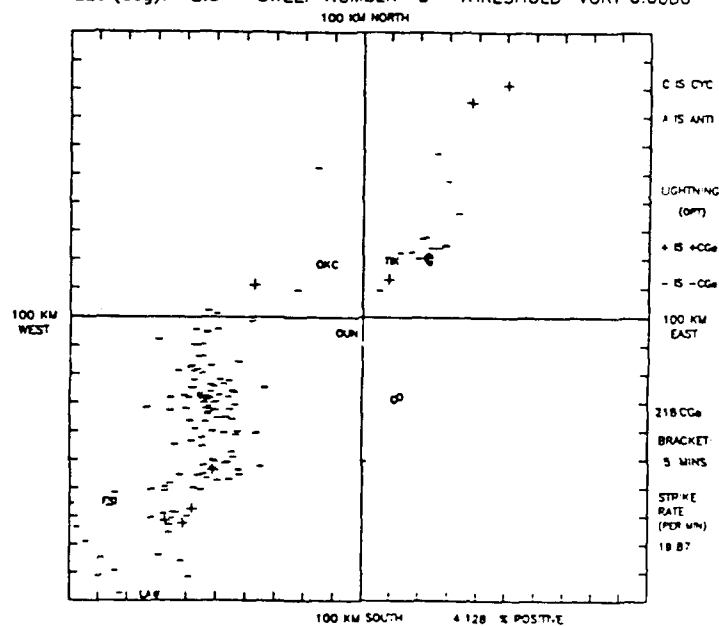
Figure 5.a.22:   Same as Figure 5.a.21 except for 0004Z (1804 CST)
on 28 May, 1987. Note lightning activity
associated with mesocyclone.
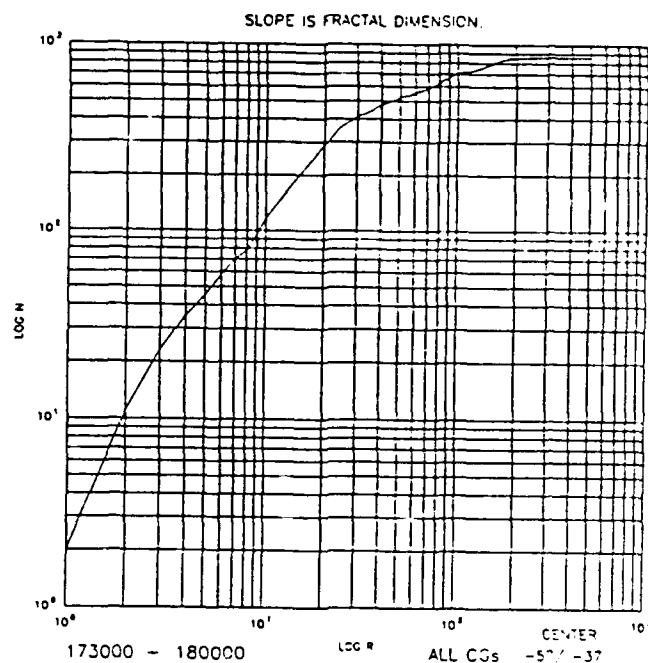
Figure 5.b.1: Representative Log/Log plot of the number of all cloud-to-ground lightning versus circle radius for a 30 minute time period. The slope of the line is the fractal dimension. Note the linear appearance.
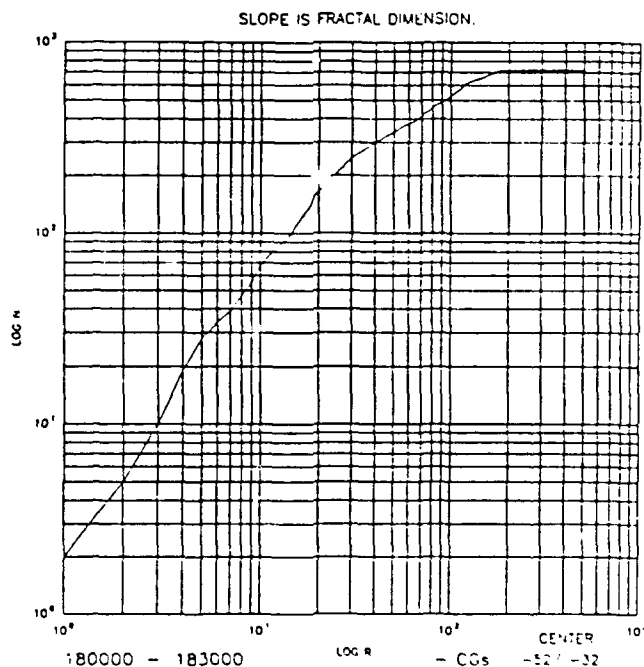
Figure 5.b.2: Same as Figure 5.b.1 except for negative cloud-to-ground lightning strikes. Note the linear appearance as well.

SLOPE IS FRACTAL DIMENSION.

153000 — 160000   +CGs   -97/-32
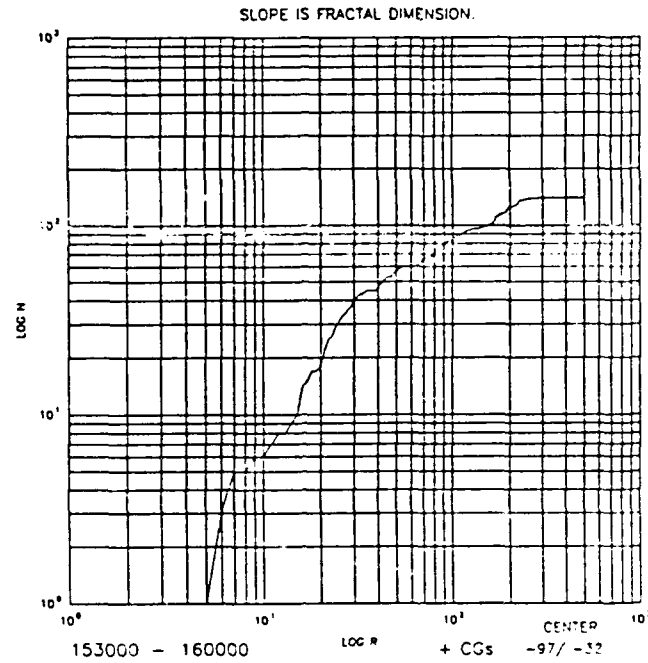
Figure 5.b.3:   Same as Figure 5.b.1 except for positive cloud-
to ground lightning strikes. Note the irreg-
ularity of the curve.

SLOPE IS FRACTAL DIMENSION.

150000 — 153000   +CGs   -47/-67
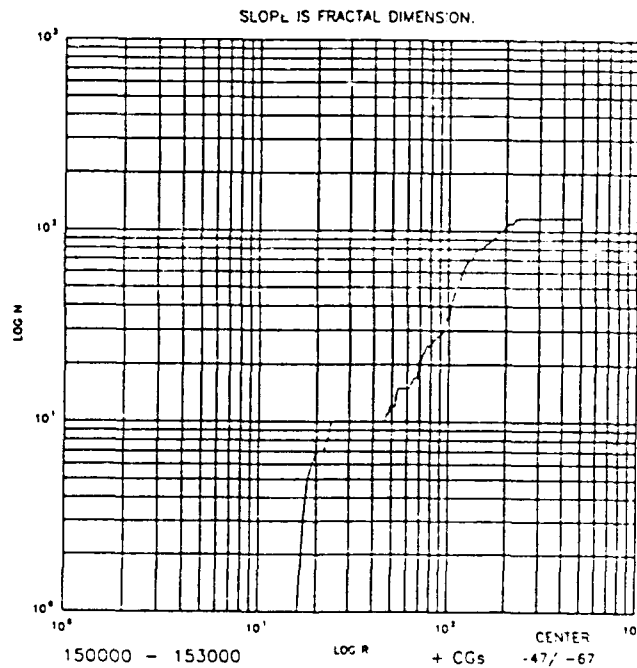
Figure 5.b.4:   Same as Figure 5.b.3. This plot has some
linearity between R=60 to R=200.

SLOPE IS FRACTAL DIMENSION.

150000 — 200000   LOG R   — CGs   -57/-37
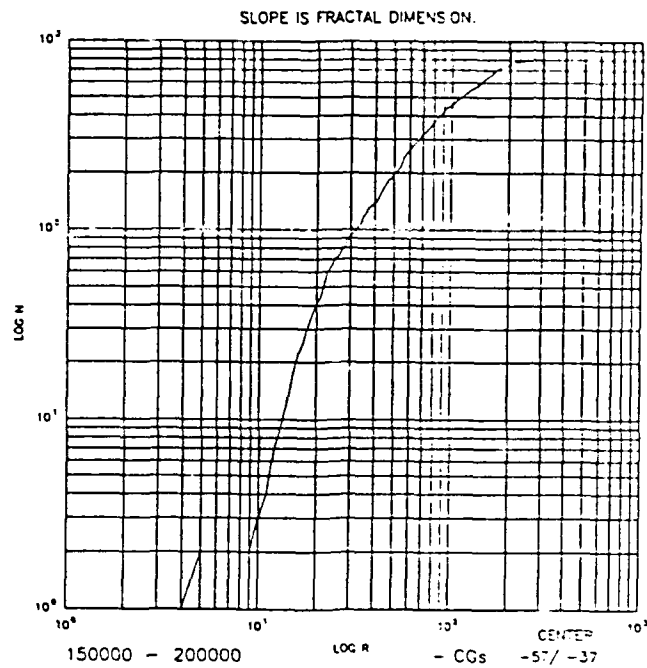
Figure 5.b.5: Same as Figure 5.b.3 except for a five hour
              time period. Note the curvature.

SLOPE IS FRACTAL DIMENSION.

150000 — 200000   LOG R   — CGs   -57/-37
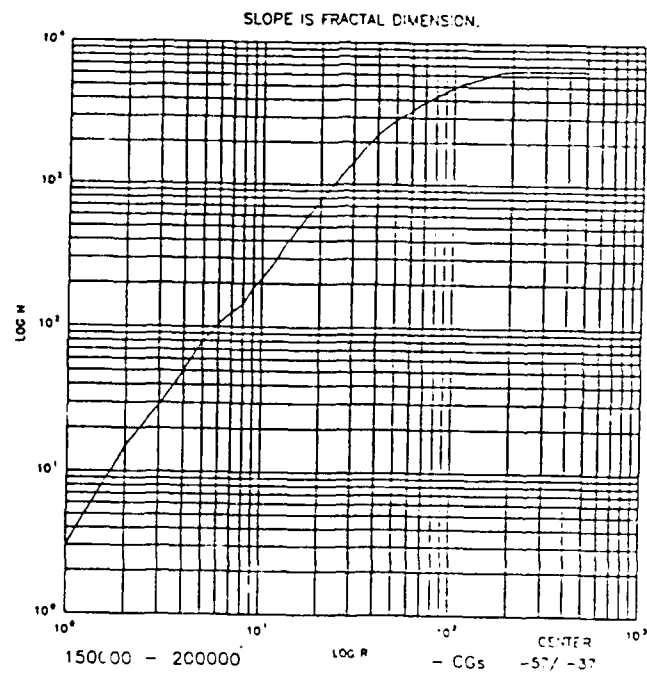
Figure 5.b.6: Same as Figure 5.b.2 except for a five hour
              time period. Note the linearity.
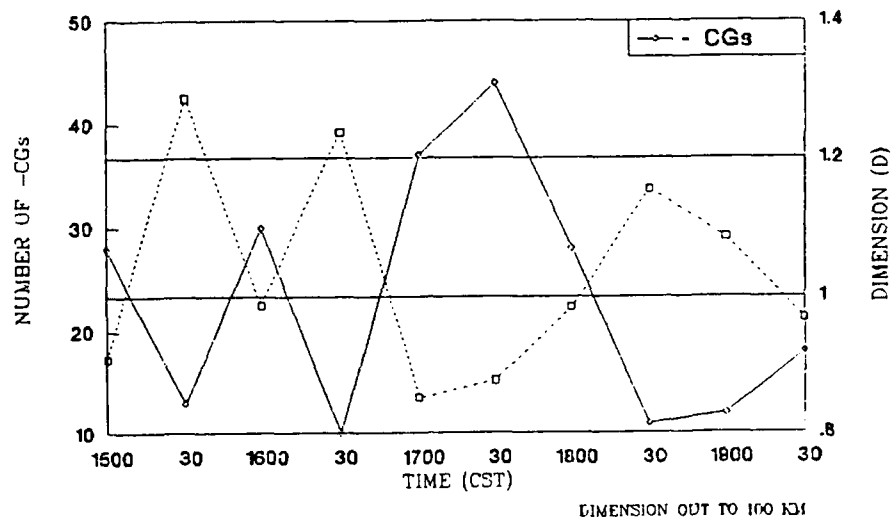
Figure 5.b.7: Plot of number of negative lightning strikes within a 5 km radius of the center (solid line) and fractal dimension (D) from center to 100 km (dashed line) versus time.
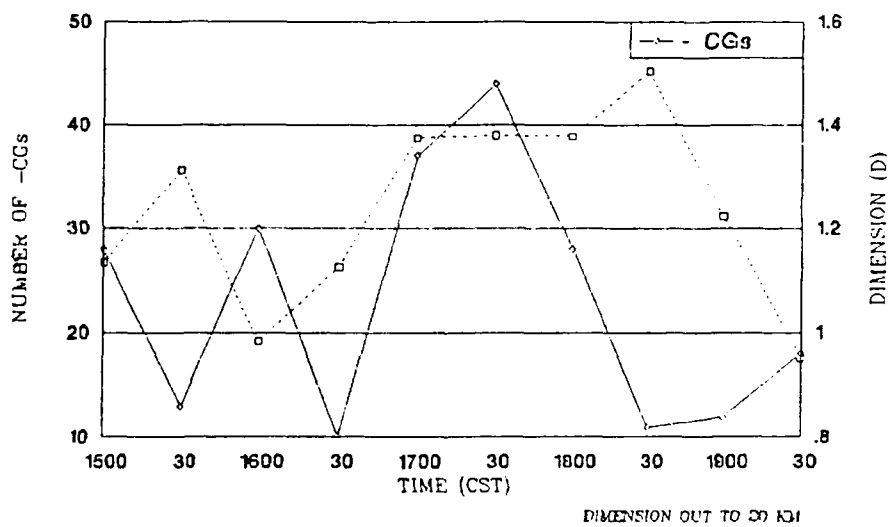
Figure 5.b.8: Same as Figure 5.b.7 except dimension (D) is from center to 20 km.

80

CHAPTER VI

NOTES ON VELOCITY ALIASING

Velocity ambiguity is an inherent problem of Doppler radar. Coupled to range, unambiguous velocity is restricted to +/- the nyquist velocity. This relationship is given by (Doviak and Zrnic, 1984):

$$RV_n = c\frac{\lambda}{8}$$

where R is unambiguous range, V_n is unambiguous or Nyquist velocity, c is the speed of light and λ is the wavelength the radar is operated at. Since the right hand side is held constant, any increase in nyquist velocity consequently reduces the range of the radar. Under normal operating conditions, some velocity "folding" is allowed in order to obtain a higher unambiguous range. For NEXRAD, a reliable method of unfolding velocities is critical to allow this new system to reach its full potential.

Many techniques have been developed to unfold or dealias Doppler velocities. They include simple one dimensional (i.e. gate-to-gate) dealiasing, two dimensional, using a

complete sweep, dealiasing (Merritt, 1984; Desrochers, 1989), local environment dealiasing which uses two adjacent radials and assumes two-dimensional continuity (Eilts and Smith, 1989) and region bridging (Albers, 1989). Many of these methods first determine a region where folding is suspected. Then an integer nyquist number (f) is chosen that will successfully dealias the data. Once the nyquist number is known, the true velocity can be obtained by (Desrochers, 1989):

$$V_t = V_m + f \times 2V_n$$

where Vt is the true velocity, Vm is the measured velocity, f is the nyquist number and Vn is the nyquist velocity. For singly folded velocity data, the nyquist number is +/- 1 and $f=0$ in areas of no aliasing.

During the course of the singularity analysis discussed in Chapters III and V, it was discovered that the singularity algorithm was well adept at locating areas where velocity aliasing had occurred. Due to the nature of velocity folding and the singularity analysis, the larger pairs of positive and negative singularity values are located near the periphery of the aliased area (see figures 6.1-2). This technique clearly delineates the region of velocity folding, a problem with current methods. Another benefit is that large nature gradient appear totally different and, therefore, can be excluded from the dealiasing process (note the gust front just east of the radar in figures 5.a.12-14).

The orientation of the singularity pattern in the folded region also gives an indication of the correct nyquist number. The pattern is arranged in pairs with convergence singularities on one side and divergence singularities on the other. The environmental flow is from the convergent singularity side toward the divergent side.

NORMAN   RADAR   DATE: 52787   TIME: 170552-170650   CS
ELE (deg):   2.2   SWEEP NUMBER   7   THRESHOLD   DIV   0.0125
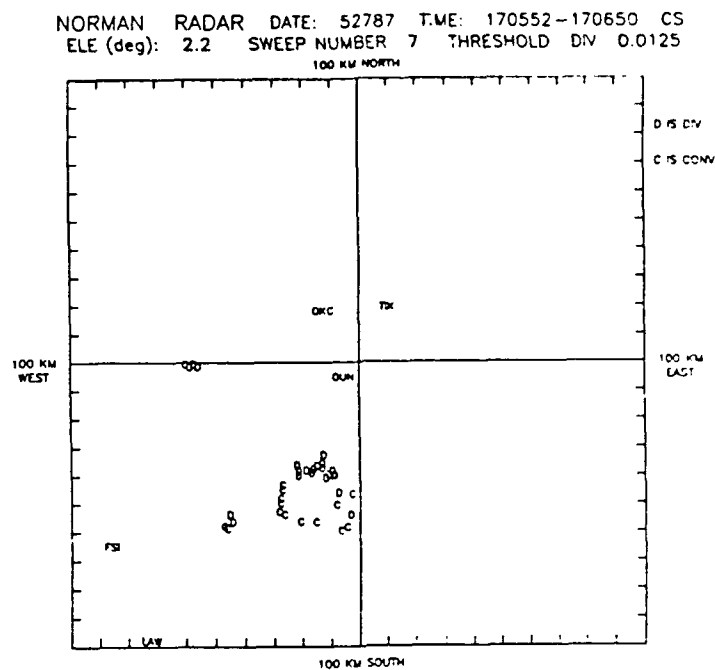
Figure 6.1: Divergence singularity display showing an area
             of folded velocities south-southwest of Norman
             (OUN). Note, with a high threshold, the singular-
             ities ring the folded velocities.

NORMAN   RADAR   DATE: 52787   TIME: 170856-170954   CS
ELE (deg):   6.2   SWEEP NUMBER   7   THRESHOLD   DIV   0.0155
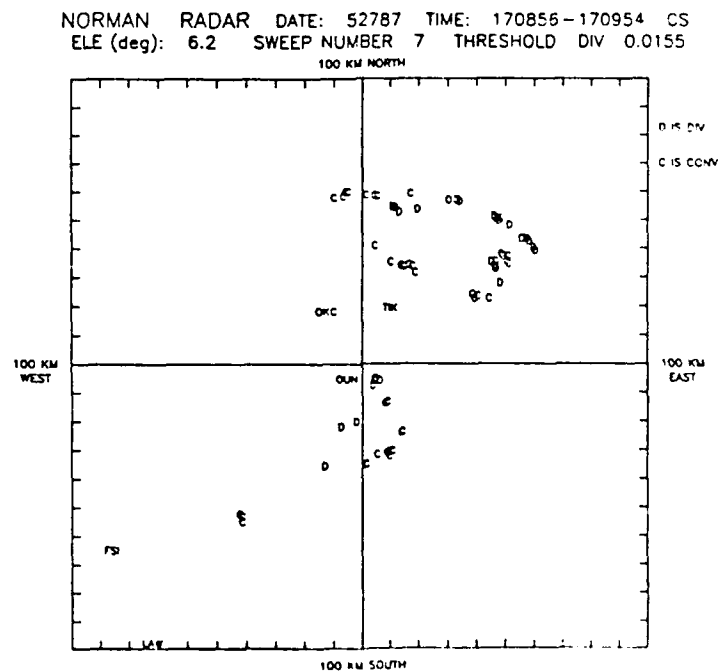
Figure 6.2: Same as Figure 6.1 except folding is northeast
             and south of Norman (OUN).

84

BIBLIOGRAPHY

Albers, S.C., 1989: Two-dimensional velocity de-aliasing in highly sheared environments, in **Preprints**, 24th Conference on Radar Meteorology, Amer. Meteor. Soc., Boston, Mass., 411-414.

Barnes, S.L., 1980: Report on a meeting to establish a common doppler radar data exchange format, **Bull. Amer. Meteor. Soc.**, **61**, 1401-1404.

Barnsley, M., 1988: **Fractals Everywhere**, Academic Press, 394 pp.

Barnsley, M.F., R.L. Devaney, B.B. Mandelbrot, H.-O. Peitgen, D. Saupe and R.F. Voss, 1988: **The Science of Fractal Images**, Springer-Verlag, 312 pp.

Beasley, W.H., M.A. Uman, D.M. Jordan, and C. Ganesh, 1983: Positive cloud to ground lightning return strokes, **J. of Geophys. Res.**, **88**, 8475-8482.

Beasley, W.H., 1985: Positive cloud-to-ground lightning observations, **J. Geophys. Res.**, **90**, 6131-6138.

Blumen, A., G. Zumofen and J. Klafter, 1988: in **Fractals, Quasicrystals, Chaos, Knots and Algebraic Quantum Mechanics**, ed. A. Amann, L. Cederbaum and W. Gans, Kluwer Academic Publishers, 331 pp.

Brook M., M. Nakano, P. Krehbiel and T. Takeuti, 1982: The electrical structure of the Hokurika winter thunderstorms, **J. of Geophys. Res.**, 87, 1207-1215.

Brook, M., R.W. Henderson and R.B. Pyle, 1989: Positive lightning strokes to ground, **J. Geophys. Res.**, 94, 13,295-13,303.

Cieslik, B.L., 1990: An application of singularity analysis to a heavy precipitation event, Master's Thesis, The University of Oklahoma, Norman Ok, 87 pp.

Cooray V., and S. Lundquist, 1982: On the characteristics of some radiation fields from lightning and their possible origin in positive ground flashes, **J. Geophys. Res.**, 87, 11,203-11,214.

Desrochers, P.R., 1989: A reliable method for real-time velocity unfolding, in **Preprints**, 24th Conference on Radar Meteorology, Amer. Meteor. Soc., Boston, Mass., 415-418.

Doviak, R.J., and D.S. Zrnic, 1984: **Doppler radar and weather observations**, Academic Press, 458 pp.

Eilts, M.D. and S.D. Smith, 1989: Efficient dealiasing of
   doppler velocities using local environment constraints, in
   Preprints, 24th. Conference on Radar Meteorology, Amer.
   Meteor. Soc., Boston, Mass., 194-197.

Engholm, C.D., E.R. Williams and R.M. Dole, 1990: Meteoro-
   logical and electrical conditions associated with positive
   cloud-to-ground lightning, **Mon. Weather Rev.**, 118,
   470-487.

Fuquay, D.M., 1982: Positive cloud-to-ground lightning in
   summer thunderstorms, **J. Geophys. Res.**, 87, 7131-7140.

Goodman, S.J. and D.R. MacGorman, 1986: Cloud-to-ground ac-
   tivity in mesoscale convective complexes, **Mon. Weather
   Rev.**, 114, 2320-2328.

Krider, E.P., R.C. Noggle and M.A. Uman, 1976: A gated wide-
   band magnetic direction finder for lightning return
   strikes, **J. Appl. Meteor.**, 15, 301-306.

Krider, E.P., R.C. Noggle, A.E. Pifer, and D.L. Vance, 1980:
   Lightning direction-finder for forest fire detection,
   Bull. Amer. Meteor. Soc., 61, 980-986.

Lamb, H., 1932: **Hydrodynamics**. Cambridge University Press.

Lovejoy, S., 1982: Area-perimeter relation for rain and
   cloud areas, **Science**, 216, 185-187.

Lovejoy, S. and D. Schertzer, 1986: Scale invariance, symmetries, fractals, and stochastic simulations of atmospheric phenomena, **Bull. Amer. Meteor. Soc.**, 67, 21-32.

MacGorman, D.R., 1990: Personal communication.

MacGorman, D.R., 1989: Class notes form **Atmospheric Electricity**, Fall 1989, Univ. of Oklahoma School of Meteorology.

MacGorman, D.R. and W.L. Taylor, 1989: Positive cloud-to-ground lightning detection by a direction-finder network, **J. Geophys. Res.**, 94, 13,313-13,318.

Mach, D.M., D.R. MacGorman, W.D. Rust and R.T. Arnold, 1986: Site errors and detection efficiency in a magnetic direction-finder network for lightning strikes to ground, **J. Atmos. Oceanic Technol.**, 3, 67-74.

Maddox, R.A., 1980: Mesoscale convective complexes, **Bull. Amer. Meteor. Soc.**, 61, 1374-1387.

Maddox, R.A., 1983: Large-scale meteorological conditions associated with midlatitude, mesoscale convective complexes, **Mon. Weather Rev.**, 111, 1475-1493.

Mazur, V., J.C. Gerlach and W.D. Rust, 1984: Lightning flash density versus altitude and storm structure from observations with UHF- and S-band radars, **Geophys. Res. Letters**, 11, 61-64.

Merritt, M.W., 1984: Automatic velocity de-aliasing of for real-time application, in **Preprints**, 22nd Conference on Radar Meteorology, Amer. Meteor. Soc., Boston, Mass., 528-533.

Milne-Thomson, L.M., 1960: **Theoretical Hydrodynamics**. The Macmillan Co., New York, 600 pp.

Newman, W.R., 1971: The relationship between horizontal moisture convergence and severe storm occurrences, Master's thesis, The University of Oklahoma, Norman, Ok, 51 pp.

Orville, R.E., R.A. Weisman, R.B. Pyle, R.W. Henderson, and R.E. Orville, Jr., 1987: Cloud-to-ground lightning flash characteristics from June 1984 through May 1985, **J. Geophys. Res.**, **92**, 5640-5644.

Orville, R.E., R.W. Henderson and L.F. Bosart, 1988: Bipole patterns revealed by lightning locations in mesoscale storm systems, **Geophys. Res. Lett.**, 15, 129-132.

Prandtl, L. and O.G. Tiejens, 1957: **Applied hydro & aeromechanics**, Dover Publications, New York, New York, 311 pp.

Reap, R.M., and D.R. MacGorman, 1989: Cloud-to-ground lightning: Climatological characteristics and relationships to model fields, radar observations, and severe local storms, **Mon. Weather Rev.**, 117, 518-535.

Rouse, H., 1961: **Fluid mechanics for hydraulic engineers**, Dover Publications, New York, New York, 422 pp.

Rust, W.D. and D.R. MacGorman, 1988: in **Thunderstorm Morphology and Dynamics**, ed. E. Kessler, Univ. of Oklahoma Press, Norman, Okla., 268 pp.

Rust, W.D., D.R. MacGorman, and R.T. Arnold, 1981: Positive cloud-to-ground lightning flashes in severe storms, **Geophys. Res. Lett.**, 8, 7, 791-794.

Rust, W.D., D.R. MacGorman and S.J. Goodman, 1985a: Unusual positive cloud-to-ground lightning in Oklahoma storms on 13 may 1983, in **Preprints**, 14th. Conference on Severe Local Storms, Amer. Meteor. Soc., Boston, Mass., 372-375.

Rust, W.D., D.R. MacGorman and W.L. Taylor, 1985b: Photographic verification of continuing current in positive cloud-to-ground flashes, **J. Geophys. Res.**, 90, 6144-6146.

Rust, W.D., 1989: Utilization of a mobile laboratory for storm electricity measurements, **J. Geophys. Res.**, **94**, 13,305-13,311.

Rutledge, S.A. and D.R. MacGorman, 1988: Cloud-to-ground activity in the 10-11 June mesoscale convective system observed during the Oklahoma-Kansas PRE-STORM project, **Mon. Weather Rev.**, **116**, 1393-1408.

Rutledge, S.A. and D.R. MacGorman, 1989: observations of positive cloud-to-ground lightning flashes from mesoscale convective systems, **Preprints**, 24th. Conference on Radar Meteorology, Amer. Meteor. Soc., Boston, Mass., 122-125.

Sasaki, Y.K., 1955: A fundamental study of the numerical prediction based on the variational principle, **J. Meteor. Soc. Japan**, **33**, 262-275.

Sasaki, Y.K., K. Mizuno, S. Allen, V. Whitehead, and K.E. Wilk, 1989: Optimized variational analysis scheme of single doppler radar wind data, **Preprints**, 3rd. International Conference on the Aviation Weather System, Anaheim, California, 9-14.

Sasaki, Y.K., B.J. Tilly and J.T. Johnson, 1990: Microburst detection by singularity analysis of a 10 cm doppler radar wind data, Manuscript prepared for publication.

Storm Data, 1987, **29**, 68 pp.

Takayasu, H., 1986: **Fractals**, Asakura Publishing Company, Tokyo, Japan, 186 pp.

Takeuti, T., M. Nakano, M. Brook, D.J. Raymond, and P. Krehbiel, 1978: The anomalous winter thunderstorms of the Hokuriku coast, **J. Geophys. Res.**, **83**, 2385-2394.

Williams, E.R., C.M. Cooke and K.A. Wright, 1985: Electrical discharge propagation in and around space charge clouds, **J. Geophys. Res.**, **90**, 6059-6070.

Williams, E.R., 1989: The tripole structure of thunderstorms, **J. Geophys. Res.**, **94**, 13,151-13,167.

Williams, E.R., M.E. Weber and R.E. Orville, 1989: The relationship between lightning type and convective states of thunderclouds, **J. Geophys. Res.**, **94**, 13,213-13,220.